Int J Physiol Pathophysiol Pharmacol 2024;16(3):28-54
www.ijppp.org /ISSN:1944-8171/IJPPP0156195

Original Article

Association of connexin36 with adherens junctions at mixed synapses and distinguishing electrophysiological features of those at mossy fiber terminals in rat ventral hippocampus

Deepthi Thomas[1], Antonia Recabal-Beyer[1,2], Joanne MM Senecal[1], Demitre Serletis[3], Bruce D Lynn[1], Michael F Jackson[4,5], James I Nagy[1]

[1]Department of Physiology and Pathophysiology, Rady Faculty of Health Sciences, Max Rady College of Medicine, University of Manitoba, Winnipeg, Manitoba, Canada; [2]Departamento de Biología Celular, Facultad de Ciencias Biológicas, Universidad de Concepción, Víctor Lamas 1290, Casilla 160, Concepción, Chile; [3]Epilepsy Center, Neurological Institute, Cleveland Clinic, Cleveland, Ohio, USA; [4]Department of Pharmacology and Therapeutics, Rady Faculty of Health Sciences, Max Rady College of Medicine, University of Manitoba, Winnipeg, Manitoba, Canada; [5]PrairieNeuro Research Centre, Kleysen Institute for Advanced Medicine, Health Science Centre, Winnipeg, Manitoba, Canada

Received February 28, 2024; Accepted May 6, 2024; Epub June 15, 2024; Published June 30, 2024

Abstract: Background: Granule cells in the hippocampus project axons to hippocampal CA3 pyramidal cells where they form large mossy fiber terminals. We have reported that these terminals contain the gap junction protein connexin36 (Cx36) specifically in the stratum lucidum of rat ventral hippocampus, thus creating morphologically mixed synapses that have the potential for dual chemical/electrical transmission. Methodology: Here, we used various approaches to characterize molecular and electrophysiological relationships between the Cx36-containing gap junctions at mossy fiber terminals and their postsynaptic elements and to examine molecular relationships at mixed synapses in the brainstem. Results: In rat and human ventral hippocampus, many of these terminals, identified by their selective expression of vesicular zinc transporter-3 (ZnT3), displayed multiple, immunofluorescent Cx36-puncta representing gap junctions, which were absent at mossy fiber terminals in the dorsal hippocampus. In rat, these were found in close proximity to the protein constituents of adherens junctions (i.e., N-cadherin and nectin-1) that are structural hallmarks of mossy fiber terminals, linking these terminals to the dendritic shafts of CA3 pyramidal cells, thus indicating the loci of gap junctions at these contacts. Cx36-puncta were also associated with adherens junctions at mixed synapses in the brainstem, supporting emerging views of the structural organization of the adherens junction-neuronal gap junction complex. Electrophysiologically induced long-term potentiation (LTP) of field responses evoked by mossy fiber stimulation was greater in the ventral than dorsal hippocampus. Conclusions: The electrical component of transmission at mossy fiber terminals may contribute to enhanced LTP responses in the ventral hippocampus.

Keywords: Gap junctions, mixed chemical/electrical synapses, electrical coupling, hippocampus, brainstem, neurotransmission, long-term potentiation, immunofluorescence

Introduction

While chemical synapses are the major form of communication between neurons, electrical synapses are also widespread functionally operative components that contribute to neuronal communication in circuitry of most major structures in the mammalian central nervous system (CNS) and that often interact with chemical synapses to mediate complex integrative functions [1-6]. These synapses are formed by gap junctions composed of connexins that form hexamers (connexons) in plasma membranes [7, 8]. Clusters of connexons in apposing membranes dock to create intercellular pores that allow cell-to-cell passage of ions and small molecules, thus creating pathways for current flow between neurons [9]. Among the family of twen-

https://doi.org/10.62347/RTMH4490

ty connexins, several are known to form electrical synapses in restricted CNS areas, but connexin36 (Cx36) is the most widely expressed in neurons of adult as well as developing brain and spinal cord [5, 10, 11] and is the constituent of the vast majority of neuronal gap junctions (nGJs) that have been identified ultrastructurally [12-17] or by other means [18, 19]. Similar to the structural and functional diversity of chemical synapses, electrical synapses have a variety of distinguishing features reflected by their multiplicity of subcellular localizations and frequent occurrence between inhibitory neurons, less frequently between excitatory neurons and more rarely between excitatory and inhibitory neurons [5]. Electrical synapses also share in common with chemical synapses their now recognized highly dynamic nature, such that they exhibit plasticity of their synaptic strength, which is imparted by various well understood and some yet to be defined modes of regulation [3, 20-25]. And finally, just as chemical synaptic transmission is supported by complex molecular machinery, so too electrical synapses are not just composed of connexin aggregates but are emerging to consist of a composite of structural, scaffolding and regulatory proteins. Some components of this complex appear to be linked with intracellular signalling pathways, while others are components of adherens junctions, which all form what we have referred to as the adherens junction-neuronal gap junction complex (AJ-nGJ complex) [5, 26-30]. All of these properties of electrical synapses critically impact on the qualitative and quantitative influence they have on information flow in circuits in which they are embedded and more generally on CNS network activity [2, 4-6, 24].

One brain area that best exemplifies the diverse cellular and subcellular deployment of nGJs and their contribution to electrical synaptic transmission is the hippocampus. Among the best characterized electrical synapses are those between various classes of hippocampal interneurons, where they contribute to the generation of high frequency oscillations, among other functions [1, 31-33]. Evidence of coupling is also found between the somata and/or dendrites of CA1 and between those of CA3 hippocampal principal cells [34, 35]. Nevertheless, Cx36 mRNA expression was found only in CA3 pyramidal cells [10] and ultrastructurally-identified gap junctions between dendritic arbors or somata of CA1/CA3 principal cells have yet to be definitively found. Yet another site of electrical coupling between pyramidal cells, inferred from various approaches, is the occurrence of gap junctions between their initial axon segments [36, 37]. More recently, we have shown immunofluorescence labelling of Cx36 localized to glutamatergic mossy fiber terminals in the stratum lucidum of rat ventral hippocampus, rendering these terminals morphologically mixed synapses with potential for dual chemical and electrical transmission [38]. This observation is consistent with ultrastructural detection of Cx36 at gap junctions along mossy fiber axons and at excitatory nerve terminals in rat hippocampus by freeze-fracture replica immunogold labelling (FRIL) [39, 40], notwithstanding that those terminals could not be definitively identified as belonging to mossy fiber terminals [40]. In addition, electrophysiological studies have provided some support for functionally operative electrical transmission at these terminals [41-43]. Some of the above findings warrant further investigation to better define the degree to which electrical synapses are extant in hippocampal neuronal circuitry and ultimately to understand their functional contributions to network activity. In particular, knowledge surrounding the mixed synapses of rat hippocampal mossy fiber terminals remains rudimentary. Here, we use immunofluorescence approaches to investigate distinguishing molecular features of those synapses as well as similar mixed synapses in the rat brainstem, and we inspect the human ventral hippocampus for association of Cx36 with mossy fiber terminals. Further, we examine electrophysiological properties of neurotransmission at mossy terminals in ventral hippocampus that contain mixed synapses vs. dorsal hippocampus where such synapses are absent.

Materials and methods

Animals and antibodies

Animals used in this study included a total of forty-five adult male Sprague-Dawley rats greater than two months of age and weighing 200 to 275 g, and eight adult male wild-type C57 BL/6-129SvEv mice greater than six weeks of age and weighing 25 to 30 g. Both rats and mice were used because data from early literature

Table 1. Primary antibodies used for immunofluorescence labelling, with type, species in which they were produced, designated catalogue number by supplier, dilution employed in this study and commercial source

Antibody	Type	Species	Designation	Dilution	Source*
Cx36	Monoclonal	Mouse	39-4200	2-4 µg/ml	ThermoFisher
ZnT3	Polyclonal	Guinea pig	197 004	1:200	Synaptic Systems
Parvalbumin	Polyclonal	Guinea pig	195 004	1:100	Synaptic Systems
N-cadherin	Polyclonal	Sheep	AF6426	2 µg/ml	R&D Systems
Nectin-1	Polyclonal	Rabbit	SC-28639	1:50	Santa Cruz
MAP2	Polyclonal	Chicken	AB2138173	1:600	EnCor Biotech
ZO-1	Polyclonal	Rabbit	61-7300	4 µg/ml	ThermoFisher

*Addresses of commercial sources are as follows: ThermoFisher, Rockford, IL, USA; Synaptic Systems, Goettingen, Germany; R&D Systems, Minneapolis, MN, USA; Santa Cruz, Dallas, TX, USA; EnCor Biotechnology Inc., Gainesville, FL, USA.

related to the present work were derived from rat tissues, and more recent similarly related studies involved the use of mice. Animals were obtained from the Central Animal Care Services at the University of Manitoba and utilized according to approved protocols by the Central Animal Care Committee of the University of Manitoba. While we use wild-type C57 BL/6-129SvEv in the present study, similar results were obtained using CD1 and C57/BL6 mouse strains. Rats and mice were housed with exposure to a twelve hr light/dark cycle, with food and water freely available, and all efforts were made to minimize animal suffering and the number of animals used. Tissues from some animals were taken for use in other studies, thereby contributing to a reduction of the total number of mice and rats used by laboratory personnel in various unrelated studies.

Immunofluorescence studies were conducted with the list of monoclonal and polyclonal primary antibodies given in **Table 1**, with western blotting and/or immunolabelling validation of antibody specificity for target proteins provided by the commercial supplier. A monoclonal anti-Cx36 antibody (ThermoFisher, Rockford, IL, USA) has been previously characterized for detection specificity of Cx36, which was confirmed using wild-type *vs*. Cx36 null mice [15, 16, 26, 44]. Secondary antibodies all produced in donkey included Cy5-conjugated anti-guinea pig diluted 1:500 (Jackson ImmunoResearch Laboratories, West Grove, PA, USA), Cy3-conjugated anti-mouse diluted 1:600 (Jackson ImmunoResearch Laboratories), and Alexa Fluor 488-conjugated anti-chicken, anti-guinea pig, anti-sheep and anti-rabbit each diluted 1:600 (Molecular Probes, Eugene, OR, USA). All primary and secondary antibodies were diluted in 50 mM Tris-HCl, pH 7.4, containing 1.5% sodium chloride (TBS) and 0.3% Triton X-100 (TBST), which additionally contained 10% normal donkey serum.

Tissue preparation

Rats and mice were sacrificed by intraperotoneal injection of an anaesthetic overdose of equithesin (3 ml/kg), placed on a bed of ice, and perfused transcardially with 25 ml of cold (4°C) pre-fixative containing 50 mM sodium phosphate buffer (pH 7.4), 0.1% sodium nitrite, 0.9% NaCl, and 1 unit/ml heparin, using a total volume of 3 ml for mice and 25 ml for rats. This was followed by perfusion with cold (4°C) fixative containing 0.16 mM sodium phosphate buffer (pH 7.4), 0.2% picric acid, and either 1%, 2% or 4% formaldehyde that was prepared by diluting a stock 20% solution of formaldehyde stored in sealed ampules (Electron Microscopy Sciences, Hatfield, PA, USA). Mice were perfused with a fixative volume of 40 ml, and rats with a volume of 100 to 150 ml. In the final step, animals were perfused with a cold (4°C) solution containing 10% sucrose in 25 mM sodium phosphate buffer (pH 7.4) to reduce excessive fixation. Brains were removed and stored at 4°C for 24 to 48 hr in cryoprotectant containing 25 mM sodium phosphate buffer (pH 7.4), 10% sucrose and 0.04% sodium azide. In a second fixation method, rats were anesthetized with isoflurane, decapitated and brains were removed and placed into ice-cold oxygenated (5% CO_2, 95% O_2) standard artificial cerebrospinal fluid (aCSF) (in mmol/l: 124 NaCl, 3 KCl, 1.3 $MgCl_2$, 2.6 $CaCl_2$, 1.25

NaH_2PO_4, 26 $NaHCO_3$ and 10 D-glucose; osmolarity adjusted to 300-310 mOsM). Hippocampi were then dissected and transverse slices of 350 µm were cut using a vibratome (Campden 7000 smz[2]). The slices were stored in aCSF for 30 min at 32°C and then transferred to aCSF at room temperature for 1 hr. Free-floating slices were then immersion fixed for 8 min in fixative solution containing 1% formaldehyde described above and stored in the cryoprotectant solution as above. This second fixation method was undertaken to allow immunohistochemical analyses of hippocampal tissue that otherwise would have been taken for electrophysiological studies.

For studies involving human hippocampal tissue, patients diagnosed with intractable epileptic seizures secondary to mesial temporal sclerosis and awaiting elective surgical resection of lesional hippocampal tissue were identified and consented for research use of resected tissue prior to surgery. The protocol for research use of resected human hippocampal tissue was approved by the Internal Review Board for ethics compliance at the Health Sciences Centre at the University of Manitoba. The use of resected tissue for research purposes did not influence in any way the manner in which the surgery would normally be performed, the time duration that it would normally require or the volume and area of tissue that would normally be resected. Following tissue procurement, no identifying information was recorded, thereby ensuring full patient confidentiality. Surgical dissection of the hippocampus was performed in standard fashion via selective hippocampectomy, at which point approximately 1 cubic inch of ventral hippocampal tissue was removed and immediately submerged into a chamber of ice-cold, oxygenated aCSF. The tissue was then sectioned using a vibratome and immersion fixed in 1% formaldehyde as above. Both perfusion fixed and immersion fixed tissues were flash-frozen, sectioned at 14 to 16 µm thickness using a cryostat, and sections were collected on gelatinized slides and stored at -40°C.

Immunofluorescence procedures

For immunofluorescence labelling, slide-mounted sections removed from storage were dried at room temperature for 10 min, and washed for 20 min in TBST. For double and triple immunofluorescence, sections were incubated for 18 to 24 hr at 4°C simultaneously with two or three primary antibodies diluted in TBST containing 10% normal donkey serum, then washed for 1 hr in TBST and incubated with appropriate secondary antibodies at room temperature for 1.5 hr. Sections were then washed in TBST for 20 min, and then in 50 mM Tris, pH 7.4, for 30 min. Some sections processed for immunolabelling were counterstained with deep red Nissl NeuroTrace (stain N21479) (Molecular Probes). All sections were coverslipped with the antifade medium Fluoromount-G (SouthernBiotech, Birmingham, AB, USA) and air-dried for 1 hr before transferring them to -20°C for long-term storage.

Immunofluorescence in tissue sections was examined and photographed by widefield and confocal microscopy using a Zeiss Imager Z2 microscope and a Zeiss Laser scanning 710 confocal microscope (LSM), and at higher resolution using a Zeiss LSM880 microscope with airyscan (Carl Zeiss Canada, Toronto, Canada) located in the Kleysen Institute for Advanced Medicine, Live Cell Imaging Facility at the university of Manitoba. Images were collected as CZI files using Zeiss Zen Black or Zen blue software (Carl Zeiss Canada). Widefield or confocal images were collected either as single scans or as z-stack images with 10 to 24 scans capturing a thickness of 4 to 8 µm of tissue at z scanning intervals of typically 0.4 µm using a 40× objective lens. Final images were assembled using CorelDraw Graphics (Corel Corp., Ottawa, Canada) and Adobe Photoshop CS software (Adobe Systems, San Jose, CA, USA). Images with Cy5 immunolabelling or deep red counterstaining were pseudocoloured either blue or white. In all figures displaying double and triple immunofluorescence labelling, panels identified by the same letters show the same fields. Proteins named in each panel are colour coded according to the fluorophore used to label the protein. Overlap of the red and green fluorophores is seen as yellow, and overlap of red, green and blue or white appears white.

Several procedures were used as search strategies for localization and quantification of numbers and sizes of Cx36-puncta in stratum lucidum and stratum radiatum. In each region examined, numerous randomly selected fields

were photographed. Each z-stack image was first viewed as a maximum intensity projection to obtain an overview of Cx36-puncta. A total of 2,593 Cx36-puncta taken from 8 images photographed from stratum lucidum and 2,701 puncta from a total of 50 images taken from the stratum radiatum region were used to examine the size difference between Cx36-puncta seen in these regions. Using Zeiss Zen software tools and raw (*i.e.,* unadjusted for displayed intensity) single scan images, the diameter of each puncta was calculated. Confocal images captured with a 40× objective lens were used to determine the number of Cx36-puncta associated with mossy fiber terminals immunolabelled for ZnT3. A total of 86 terminals with diameters ranging from 3-5 µm were examined. The overlap of labels for ZnT3 and Cx36 was examined in z-stack images by 3D rendering in transparency mode, with image rotation in x, y and z-axes to exclude cases where labels for ZnT3 and Cx36 overlapped but were separated in the z-axis, and to confirm cases where labels were found that overlapped in standard 2D views of the x and y axes, but not separated in the z-axis. Single, consecutive scan images within the compiled z-stack were then visually scrutinized at high digital image magnification to further confirm qualitatively the association of labels for ZnT3 and Cx36 in all three axes. The puncta per terminal were then counted manually. To establish significance, data were subject to unpaired two-tailed Student's t-test for samples with unequal variance. Unequal sample variance was first determined using the F-test for variance. Criterion for significance was set at $P < 0.05$. All data were expressed as means ± s.e.m. Statistical analysis was conducted using Microsoft Excel 2010 software.

Brain slice electrophysiology

Hippocampal slices were prepared from 3-4 weeks old Sprague-Dawley rats as previously described [45-48] with modifications. Hippocampi dissection and slicing were performed in N-Methyl-D-glucamine (NMDG-containing aCSF: (in mM) 93 NMDG, 3 KCl, 5 $MgCl_2$, 0.5 $CaCl_2$, 1.25 NaH_2PO_4, 30 $NaHCO_3$, 20 HEPES buffer, 25 glucose, 5 Na ascorbate, 3 Na pyruvate; pH adjusted to 7.4 with HCl, osmolarity adjusted to 300-310 mOsM. Prior to recording, slices were stored in HEPES containing aCSF: (in mM) 95 NaCl, 3 KCl, 1.3 $MgCl_2$, 2.6 $CaCl_2$, 1.25 NaH_2PO_4, 30 $NaHCO_3$, 20 HEPES, 25 glucose, 5 Na ascorbate, 3 Na pyruvate; pH adjusted to 7.4 with NaOH, osmolarity adjusted to 300-310 mOsM) for 30 min at 32°C and then at room temperature for 1 hr.

For extracellular field recordings, slices were transferred to a submersion recording chamber perfused with oxygenated aCSF at a flow rate of 3 ml/min and maintained at 30-32°C. Patch pipettes were pulled from borosilicate glass (World Precision Instruments, Inc., Sarasota, FL). fEPSPs were evoked by giving stimuli with a concentric bipolar stimulating electrode positioned beneath the cell layer of the dentate gyrus where mossy fibers from this region travel as a thick band to synapse onto CA3 pyramidal cells. The recording electrode with a pipette resistance of 2-5 MΩ was filled with aCSF and positioned within the CA3 stratum lucidum. One of the distinguishing features of the mossy fiber-CA3 response is that they show pronounced frequency facilitation (FF). The FF was measured by recording the baseline response for 2 min at 0.05 Hz, then switching to 1 Hz stimulation for 40 sec, and switching back to 0.05 Hz stimulation. A minimum of 300% increase in the field response amplitude compared with the baseline was set as a criterion for confirming that the response originated from mossy fiber stimulation. The recording and stimulating electrodes were repositioned until this minimum criterion was met. The stimulus intensity was set to evoke a field response of amplitude 0.2-0.3 mV. Also, to confirm the recorded events were generated from mossy fibers, a metabotropic glutamate transporter mGluR2 agonist, dicarboxycyclopropyl glycine (DCG-IV) (1 µM), was applied at the end of the recordings. A 75-80% reduction in the fEPSP response amplitude is considered as validation for mossy fiber response. For experiments involving long-term potentiation (LTP), 2-amino-5-phosphonopentanoic acid (APV) (50 µM) was added to the perfusion medium, and baseline fEPSPs were recorded for 20 min. A high-frequency stimulation (HFS) was given consisting of two consecutive 100 Hz stimulation trains lasting 1 sec each, with an inter-train interval of 20 sec. Responses were then recorded for 60 min, and DCG-IV was applied for 5 min at the end of the recordings. Amplitudes of the fEPSPs were normalized to the baseline and ana-

lyzed. The field potentials were amplified using Molecular Devices 200B amplifier and digitized with Digidata 1322A. The data were sampled at 10 kHz and filtered at 2 kHz. Traces were obtained by pClamp 9.2 and analyzed using Clampfit 10.7. Frequency facilitation was measured in dorsal hippocampus using 12 slices taken from 10 animals and in ventral hippocampus using 13 slices taken from 9 animals. LTP was measured in dorsal and ventral hippocampus using for each region 11 slices taken from 9 animals. To establish significance, data were subject to unpaired two-tailed Student's t-test with Welch's correction. Criterion for significance was set at $P < 0.05$. All data were expressed as means ± s.e.m. Statistical analysis was conducted using Microsoft Excel 2010 software.

Results

Cx36 localization to ZnT3⁺ mossy fiber terminals

Our previous demonstration of the association of Cx36 with mossy fiber terminals in rat hippocampus was based on the localization of immunofluorescence labelling for Cx36 at nerve terminals immunolabelled for the excitatory transmitter marker vesicular glutamate transporter1 (vglut1) in the stratum lucidum of the ventral hippocampal CA3 region, where the axons of granule cells in the dentate gyrus terminate as mossy fiber terminals [38]. In the stratum lucidum and many other CNS regions we have examined [5, 26, 44, 49-53], immunofluorescence labelling of Cx36 has an exclusively punctate appearance (*i.e.,* Cx36-puncta) and is invariably localized to the surface of neuronal elements. Intracellular labelling for Cx36 remains largely undetectable at least *in vivo*, perhaps due to rapid trafficking of Cx36 to plasma membranes leaving low levels within cells, or due to masking of Cx36 epitopes at intracellular compartments rendering them undetectable by currently available antibodies. Throughout the CNS, the localization of Cx36-puncta is well correlated with sites of ultrastructurally-defined Cx36-containing nGJs [12-16, 54, 55], and those puncta therefore serve as markers for such junctions *in vivo*. The localization of Cx36-puncta at vglut1-positive (vglut1⁺) terminals in the stratum lucidum thus represents strong evidence for the presence of nGJs at these terminals. However, vglut1 is a marker not only of mossy fiber terminals, but also other excitatory terminals within and surrounding the stratum lucidum, and nGJs have been found ultrastructurally at various types of excitatory nerve terminals in the different strata of the hippocampus [40]. Thus, to examine Cx36 localization more selectively to mossy fiber terminals, we used a marker expressed at exceptionally high levels in these terminals, namely vesicular zinc transporter3 (ZnT3) [56, 57].

An overview of immunolabelling for ZnT3 in the hippocampal hilus and stratum lucidum is shown in **Figure 1A**, and its high expression in mossy fiber terminals is shown magnified in **Figure 1B**. The typical appearance of Cx36-puncta in the stratum lucidum of the rat ventral hippocampus is shown in **Figure 1C1**, and the co-distribution of those puncta among ZnT3⁺ mossy fiber terminals is shown in **Figure 1C2**. Higher magnification confocal imaging revealed the remarkable degree to which clusters of Cx36-puncta (**Figure 1D1**) were localized at ZnT3⁺ terminals (**Figure 1D2**). With reference to hippocampal nomenclature [58, 59], where the proximal-distal regions of the CA3 subfields have been designated as CA3c, CA3b and CA3a, we previously described the highest density of Cx36-puncta associated with mossy fiber terminals in the CA3b and only a portion of the CA3c subfields and an absence in the CA3a subfield in the rat ventral hippocampus. Cx36-puncta at mossy fiber terminals were absent in all three of these subfields in the dorsal hippocampus of rat [38]. However, we now find that many ZnT3 terminals throughout the CA3b and CA3c regions of the stratum lucidum in the ventral hippocampus displayed Cx36-puncta. From counts of the proportion of those terminals containing puncta within these two fields, we found that 62 ± 6% harboured Cx36-puncta, with the remainder devoid of puncta.

To the extent that individual isolated ZnT3⁺ structures could be designated as single mossy fiber terminals in images such as shown in **Figure 1D2**, many of those structures contained at least one Cx36-punctum, but most contained several puncta. Among those ZnT3⁺ terminals displaying Cx36-puncta, analysis of numerous terminals showed that they contained an average of 2.4 ± 0.2 puncta per terminal. This is likely an underestimate because while z-stack images may have captured the

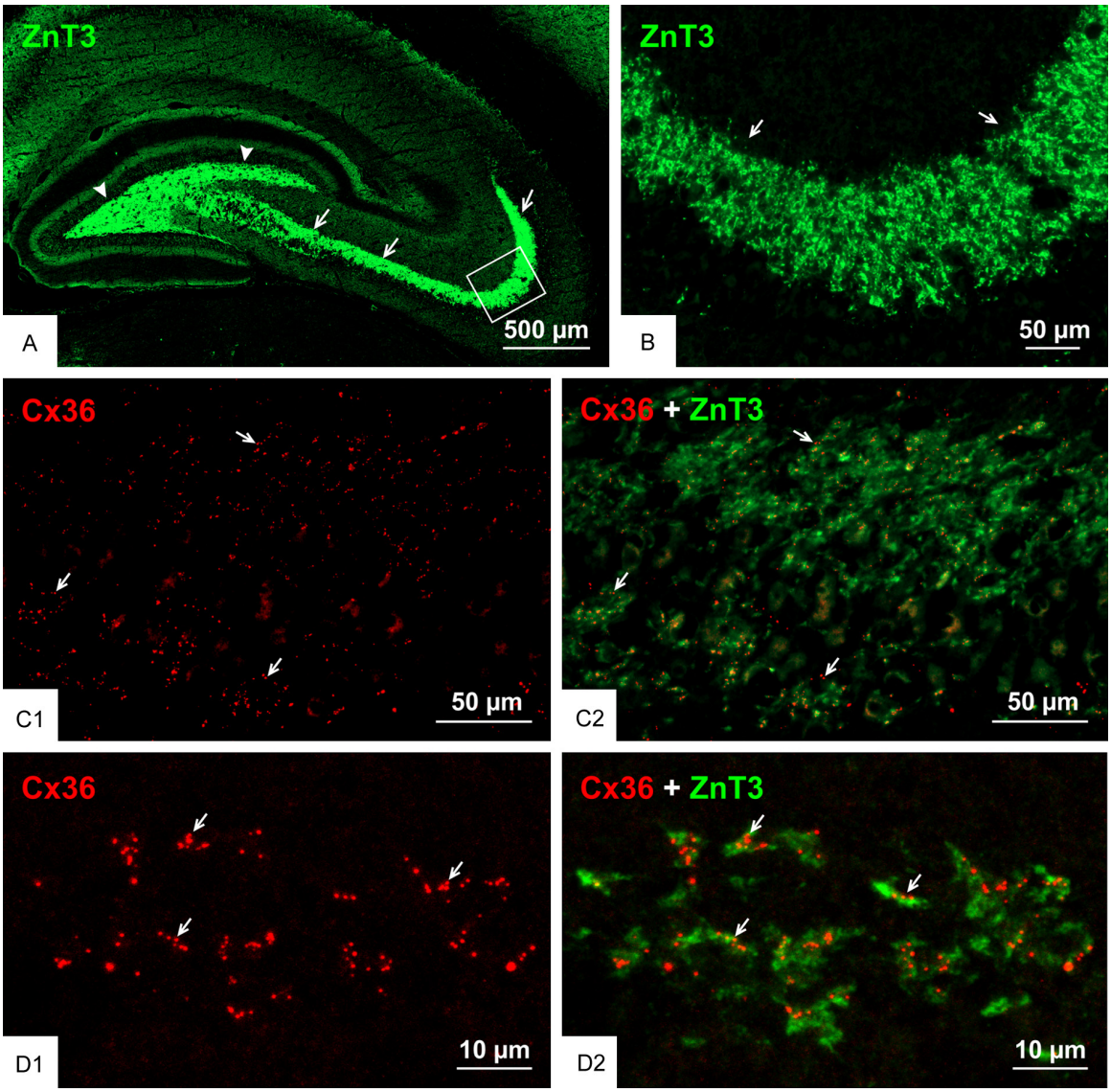

Figure 1. Association of Cx36 with ZnT3$^+$ mossy fiber terminals in adult rat ventral hippocampus. (A) The ventral hippocampus sectioned transversely along its longitudinal axis showing low magnification overview of immunofluorescence labelling for ZnT3 in the hippocampal stratum lucidum (arrows) and hilus (arrowheads). (B) Higher magnification of the boxed area in (A), showing a high density of ZnT3$^+$ mossy fiber terminals (arrows) in the stratum lucidum. (C) Double immunofluorescence labelling showing a moderate density of Cx36-puncta in the stratum lucidum of the ventral hippocampus (C1) and their association with mossy fiber terminals in this region (C2, arrows). (D) Confocal magnification of double labelling in the stratum lucidum showing clusters of Cx36-puncta (D1, arrows) localized to ZnT3$^+$ mossy fiber terminals (D2, arrows).

entirety of some mossy fiber terminals, the upper and lower extremities of those stacks could exclude out-of-field portions of terminals where Cx36-puncta may be localized, though this may be mitigated somewhat by our examination only of terminals that were 3-5 µm in diameter.

Consistent with the identification of ultrastructurally-identified nGJs in virtually all areas of the rat hippocampus [32, 40], Cx36-puncta at various densities occupied all regions of this structure. A comparison of the appearance of those in the stratum lucidum *vs.* radiatum in the ventral hippocampus is shown in **Figure 2A** and **2B**, respectively. Puncta in the stratum lucidum (**Figure 2A**) were present at high density, organized in clusters as expected given their localization to mossy fiber terminals, and displayed a wide range of sizes. In contrast,

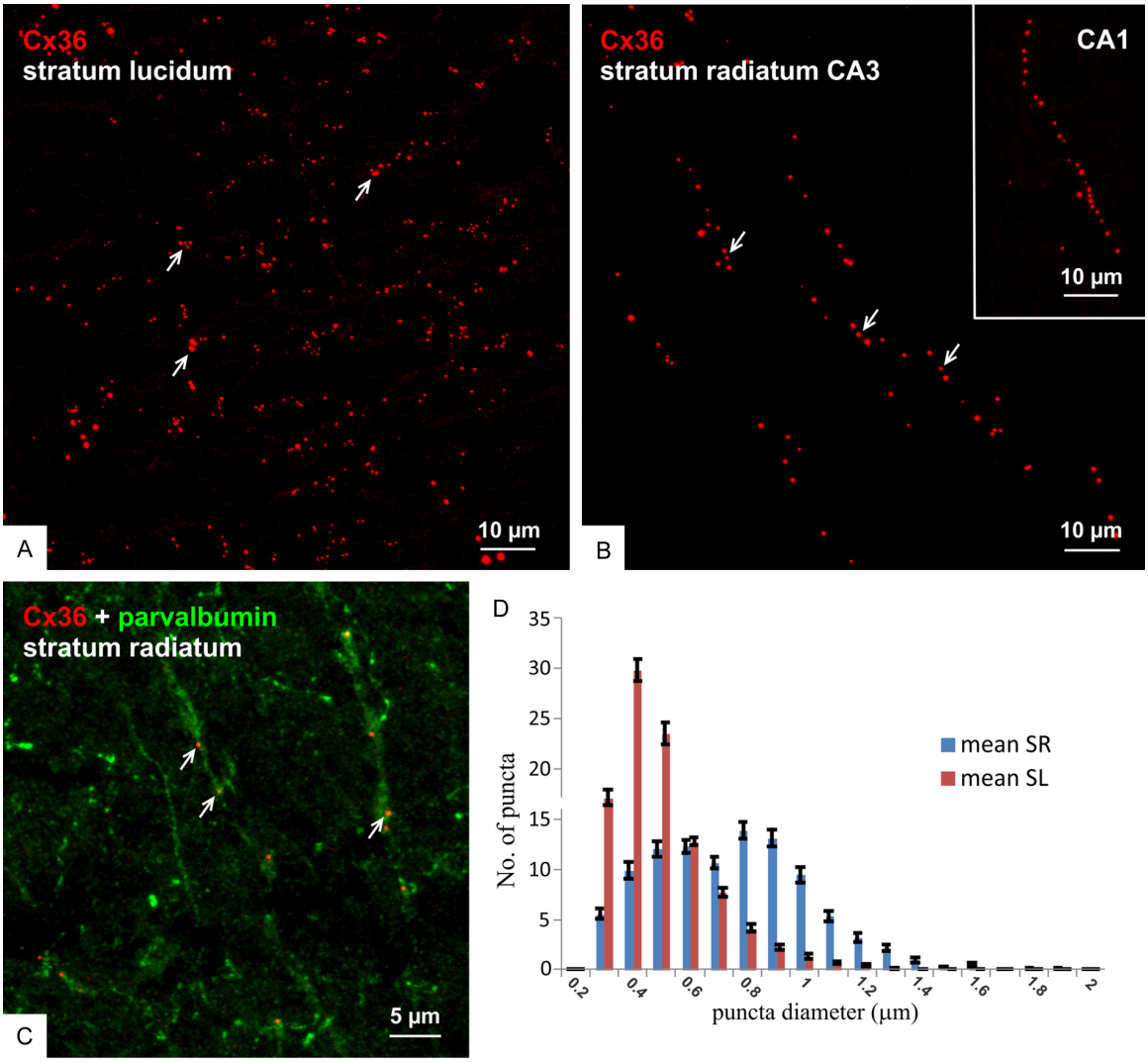

Figure 2. Distribution of Cx36-puncta in regions of adult rat ventral hippocampus. (A-C) Comparison of the appearance of immunofluorescent Cx36-puncta in the ventral stratum lucidum showing their moderate density and occurrence often in clusters (A, arrows) vs. those in the ventral stratum radiatum of the CA3 region (B) and CA1 region (B, inset) showing Cx36-puncta of generally large size and organized in linear arrays (B, arrows) along parvalbumin$^+$ dendrites (C, arrows). (D) Distribution of Cx36-puncta size in the stratum lucidum (SL) vs. stratum radiatum (SR), showing a shift to a larger diameter of those in the stratum radiatum.

Cx36-puncta in the stratum radiatum in the CA3 region (**Figure 2B**) and the CA1 region (**Figure 2B**, inset) were often arranged in linear arrays reflecting their localization along dendritic shafts, such as those of parvalbumin$^+$ interneuronal dendrites (**Figure 2C**), and tended to be of larger size than Cx36-puncta in the stratum lucidum. Measures of Cx36-puncta diameters in the two strata (**Figure 2D**) showed an average of 450 ± 0.004 nm for those in the stratum lucidum, which was significantly different from the average of 683 ± 0.005 nm for those in the stratum radiatum. This is consistent with observations by FRIL that gap junctions formed by interneurons were larger than those at excitatory mixed synapses [40]. It should be noted that these are relative measures and, due to halation incurred by immunofluorescence imaging, are not reflective of the actual much smaller sizes of nGJs as seen by both thin-section electron microscopy (EM) and FRIL [32, 40].

Granule cell collateral projections

It has been recognized that unlike other cortical principal neurons, granule cells are unique

in that they have more than one terminal type associated with their axons [60-62]. Thus, in addition to mossy fiber terminals, there are filopodial extensions and *en passant* contacts (approximately 2 μm) along mossy fibers, which synapse with inhibitory interneurons in the hippocampal hilus. Also, there are other mossy fiber expansions (3-5 μm diameter) similar to the boutons seen at CA3, which contact the dendrites and somata of excitatory mossy cells in this region [60-63]. We sought to determine whether the filopodial extensions, *en passant* terminals and the larger expansions that contact mossy cells in the hilus also form mixed synapses similar to those at mossy fiber terminals in CA3. Immunofluorescence labelling for ZnT3 was detected at very high density in the hilus of the ventral hippocampus (**Figure 3A1**; arrows in **Figure 1A**), where this labelling was presumably associated with the endings of mossy fiber collaterals that terminate in part on hilar mossy cells. In contrast, Cx36-puncta were very sparsely distributed in the ventral hilus (**Figure 3A2**), and none of the Cx36-puncta were associated with $ZnT3^+$ terminals (**Figure 3A3**), which was confirmed by rotation of z-stacked 3D images captured from 24 confocal scans. We were confident that the paucity of Cx36-puncta in the ventral hilar region was not due to ineffective labelling by examining Cx36 in a nearby region of the stratum lucidum of the same tissue section, where the density of Cx36-puncta and the association of these with mossy fiber terminals was typical of that usually seen (**Figure 3B**). Presumptive mossy cells visualized by intensely labelled $ZnT3^+$ terminal contacts on their somata located at the border between the hilus and granule cell layer (**Figure 3C1**) and having previously described morphologies [64] were also found in fields with very few Cx36-puncta (**Figure 3C2**) and these terminals were also devoid of Cx36-puncta (**Figure 3C3**). It thus appears that mossy fiber collaterals do not form mixed synapses with their postsynaptic targets.

Cx36 localization to mossy fiber terminals in human hippocampus

In our previous report on the localization of Cx36 in rodent stratum lucidum, we noted that mossy fiber terminals in both the dorsal and ventral hippocampus of mouse were devoid of labelling for Cx36 [38], thus revealing a major rat vs. mouse species difference in the synaptic composition of these terminals. While we have not yet examined Cx36 localization in the hippocampus of other sub-primate mammalian species, it was pertinent to consider whether cellular deployment of Cx36 in ventral hippocampus of human brain paralleled our findings in rat ventral hippocampus. Shown in **Figure 4** are images of resectioned ventral hippocampal tissue obtained from patients who have undergone treatment for intractable epileptic seizures. Samples from three separate patients were taken for immunolabelling, one of which was unsuccessful due to extensive secondary mesial temporal sclerosis. In the other two samples, labelling for ZnT3 in the stratum lucidum was robust and typical of that seen in rat, and this labelling was highly co-distributed with that of Cx36 (**Figure 4A**). Labelling of Cx36 had the same punctate appearance as seen throughout rat and mouse CNS, and Cx36-puncta in the stratum lucidum of human ventral hippocampus were often localized to $ZnT3^+$ mossy fiber terminals (**Figure 4B**), similar to that seen in rat. Comparison of this labelling between ventral and dorsal human hippocampus was precluded by the unavailability of dorsal hippocampal samples.

The AJ-nGJ complex at mixed synapses in hippocampus

We previously reported that nGJs referred as "purely electrical synapses" are frequently immediately adjacent to or intimately surrounded by adherens junctions linking plasma membranes, forming what we termed the AJ-nGJ complex [30]. Here, we examined whether the same is true at mixed synapses, because a similar association at these synapses could shed some light on the organization of their gap junction component based on known deployment of synaptic adherens junctions. Adherens junctions at individual mossy fiber terminals consist of rows of multiple punctate junctions, with cumulative lengths of up to 2-3 μm when viewed on-edge and corresponding diameters when viewed *en-face*, consistent with thin-section EM measures of the span encompassed by these junctional arrays [61, 65]. Adherens junctions associated with mossy fiber terminals have been the subject of intensive study and they have served as a model system to define the molecular constituents of these junctions,

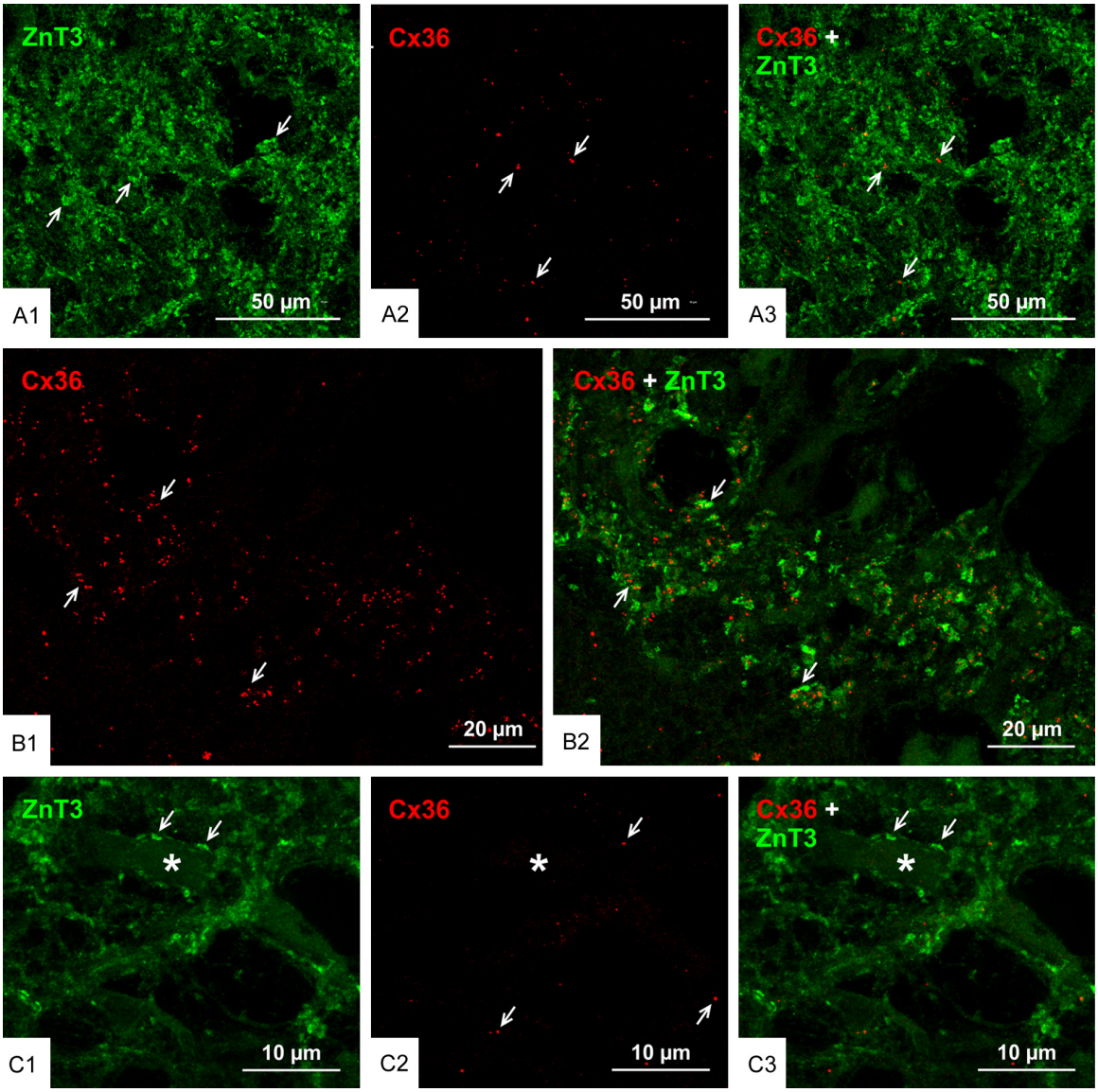

Figure 3. Paucity of Cx36-puncta among axon collaterals of mossy fibers in the ventral hippocampal hilus. (A) Double immunofluorescence labelling in a central region of the hilus showing a high concentration of ZnT3$^+$ terminals formed by axon collaterals of mossy fibers (A1, arrows) and the same field showing sparse Cx36-puncta (A2, arrows), with a lack of Cx36-puncta association with ZnT3$^+$ terminals (A3, arrows). (B) A field in the same section as imaged in (A) and serving as positive control for labelling of Cx36 with the typically moderate density of Cx36-puncta (B1, arrows) in the CA3c region of the stratum lucidum and the localization of these puncta to ZnT3$^+$ mossy fiber terminals (B2, arrows). (C) Image of a presumptive mossy cell (C1, asterisk) lying at the border between the ventral blade of the granule cell layer and the hilus, showing ZnT3$^+$ terminals on the mossy cell somata (C1, arrows) and very sparse labelling for Cx36 in the same field (C2, arrows), where ZnT3$^+$ terminals on the mossy cell lack association with Cx36-puncta (C3, arrows).

including the closely linked protein components N-cadherin and nectin-1 [66-68]. The distribution of immunofluorescence labelling for N-cadherin in various layers of rat ventral hippocampus is shown in **Figure 5A**, with a magnified region showing intense labelling for N-cadherin in the stratum lucidum (**Figure 5B**).

Triple immunofluorescence labelling of ZnT3, Cx36 and N-cadherin in the stratum lucidum is shown in **Figure 5C**. Labelling of N-cadherin appeared as long slender structures in on-edge views and ovoid or irregular shapes when viewed *en-face* or at oblique angles (**Figure 5C1**). Cx36-puncta localized to mossy fiber ter-

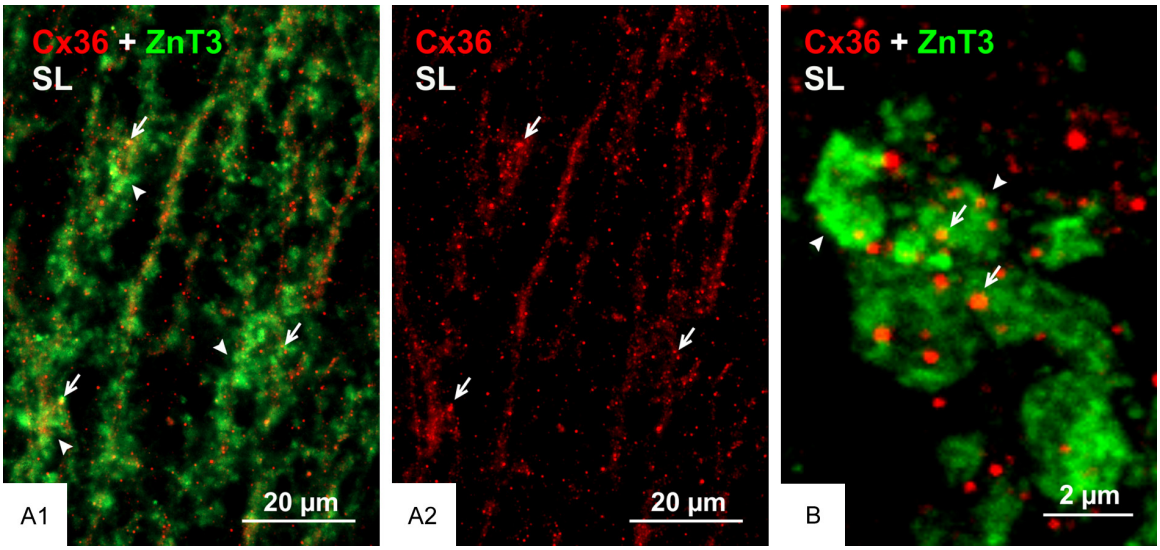

Figure 4. Immunofluorescence localization of Cx36 in the stratum lucidum of human hippocampus. (A) Overlay image showing a high density of labelling for ZnT3 at mossy fiber terminals in the stratum lucidum of ventral hippocampus and co-distribution of labelling for Cx36 (A1), which appears as Cx36-puncta of moderate density (A2). (B) Higher magnification of ZnT3$^+$ mossy fiber terminals (arrowheads) with their overlapping or closely associated Cx36-puncta (arrows).

minals (**Figure 5C2**) and labelling for N-cadherin localized to these terminals (**Figure 5C3**) were seen to be highly co-distributed, with Cx36-puncta of much smaller size than the adherens junctions associated with mossy fiber terminals often overlapping, immediately adjacent to or straddling N-cadherin$^+$ junctions (**Figure 5C4**). Similarly, triple labelling for Cx36, nectin-1 and ZnT3 showed a high density of labelling for nectin-1 in the stratum lucidum (**Figure 6A1**), with the vast majority of Cx36-puncta overlapping or straddling nectin-1$^+$ adherens junctions (**Figure 6A2**) that were localized to mossy fiber terminals (**Figure 6A3**), which is shown at higher confocal magnification in **Figure 6B**. These results indicate that maintenance of an AJ-nGJ complex is a characteristic feature of a subpopulation of mossy fiber terminals restricted to the CA3b and CA3c regions of the ventral hippocampus. Some of the larger Cx36-puncta in these fields lacked association with nectin-1 and ZnT3 and therefore may represent gap junctions localized on dendrites of interneurons as shown in **Figure 2C**, which may be devoid of or have less distinctive adherens junctions, or may express different cadherin and nectin proteins at such junctions.

We next examined the localization of Cx36-puncta and N-cadherin at the AJ-nGJ complex of mossy fiber terminals in relation to CA3 pyramidal cell dendrites labelled for the microtubule marker microtubule-associated protein2 (MAP2). Triple immunofluorescence labelling for Cx36, N-cadherin and MAP2 in the CA3b and CA3c regions of the stratum lucidum revealed numerous sites where Cx36-puncta associated with N-cadherin$^+$ adherens junctions (i.e., the AJ-nGJ complex) were localized to MAP2$^+$ dendrites (**Figure 7A**) that could often be followed back to their parent CA3 pyramidal cell bodies of origin (not shown). In images of the AJ-nGJ complex viewed on-edge, the complex was typically seen extending along one or the other dendritic peripheral border (**Figure 7B**) and occasionally along both peripheral dendritic borders (**Figure 7C**). With the AJ-nGJ complex viewed *en-face*, clusters of Cx36-puncta localized among patches of labelling for N-cadherin were seen along large MAP2$^+$ dendrites (**Figure 7D**). In the case of AJ-nGJ complexes viewed on-edge, some Cx36-puncta and their associated adherens junctions were displaced by usually less than 0.2 µm slightly outside of labelling for MAP2, which is likely due to the sparse distribution and hence low level of labelling for MAP2-associated microtubules near the plasma membranes of dendritic shafts [61, 69]. In an effort to more fully scrutinize spatial relationships between CA3 pyrami-

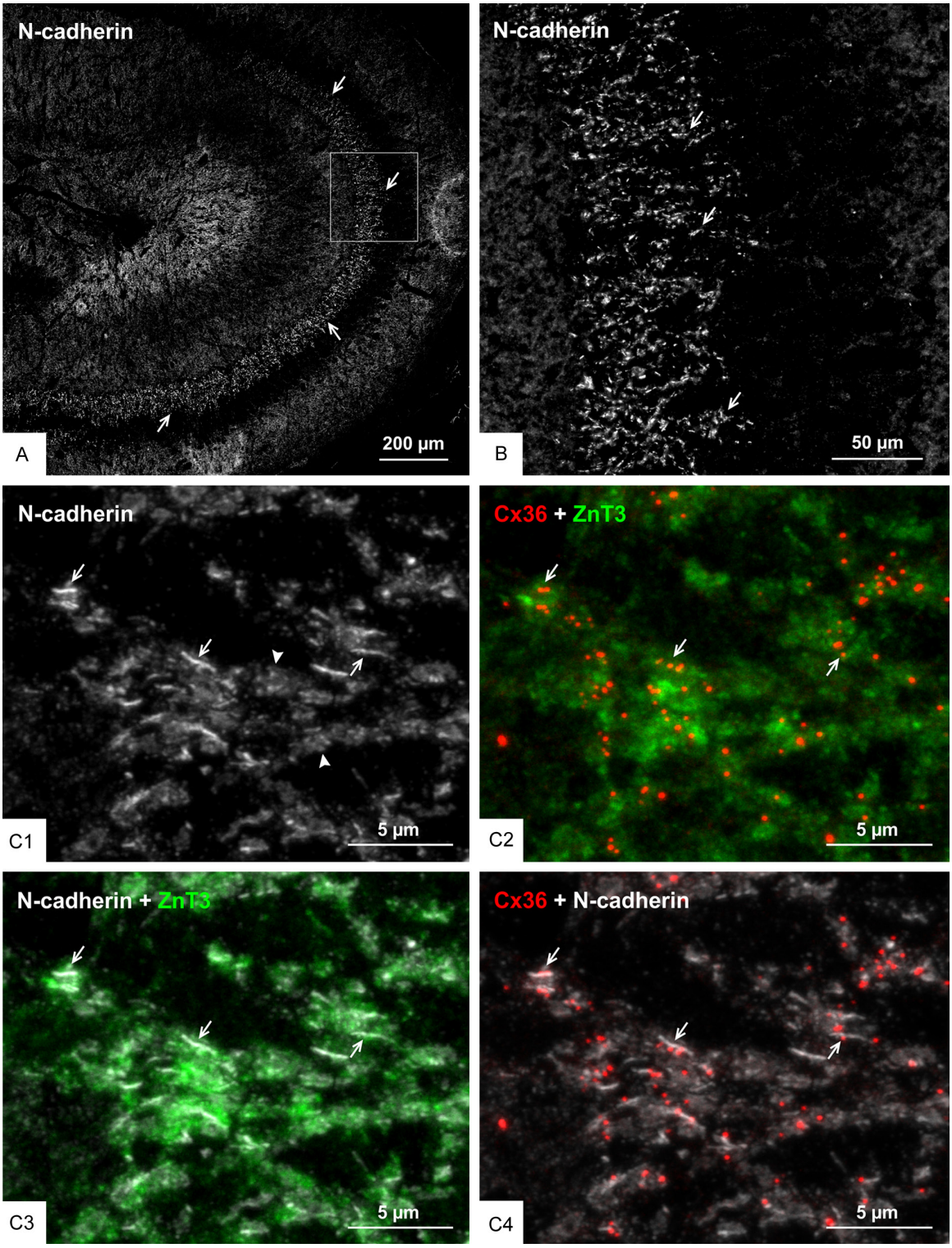

Figure 5. Association of Cx36 with N-cadherin$^+$ adherens junctions at mossy fiber terminals in adult rat ventral hippocampus. (A, B) Low magnification overview of the distribution of N-cadherin$^+$ adherens junctions in regions of the ventral hippocampus including the stratum lucidum (A, arrows), and magnification of the boxed area in (A) showing a high density of N-cadherin$^+$ adherens junctions in the stratum lucidum (B, arrows). (C) Confocal magnification of the stratum lucidum showing N-cadherin$^+$ adherens junctions seen as linear strands in on edge views (C1, arrows) and as discs in en face views (C1, arrowheads). Cx36-puncta in the same field is localized to ZnT3$^+$ mossy fiber terminals as seen in red/green overlay (C2, arrows), and N-cadherin$^+$ adherens junctions are also localized to those terminals as shown in white/green overlay (C3, arrows), with Cx36-puncta often localized at or adjacent to those junctions as shown in white/red overlay (C4, arrows).

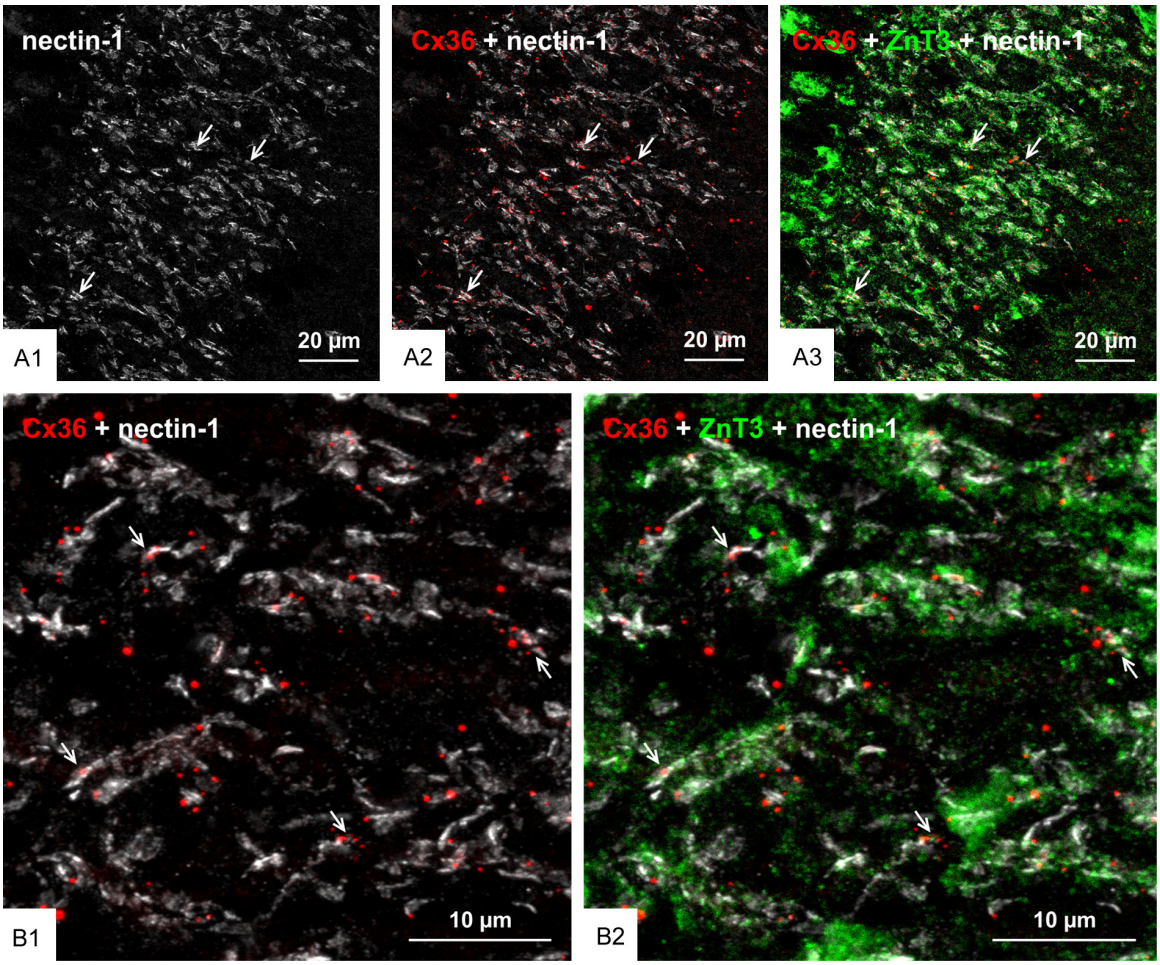

Figure 6. Association of Cx36 with nectin-1$^+$ adherens junctions at mossy fiber terminals in adult rat ventral hippocampus. (A) Low magnification overview of the distribution of nectin-1$^+$ adherens junctions in the ventral hippocampus, showing immunofluorescence labelling of nectin-1 highly concentrated in the stratum lucidum (A1, arrows), where it is co-distributed with Cx36-puncta (A2, arrows) and ZnT3$^+$ mossy fiber terminals in this region (A3, arrows). (B) Confocal magnification of a region in stratum lucidum similar to that in (A), showing the vast majority of Cx36-puncta overlapping with or immediately adjacent to nectin-1$^+$ adherens junctions (B1, arrows) localized to ZnT3$^+$ mossy fiber terminals (B2, arrows).

dal cell dendrites, adherens junctions and Cx36-puncta in the stratum lucidum, we used the higher resolution capabilities of confocal airy-scan optics. With this approach, adherens junctions immediately adjacent to CA3 pyramidal cell proximal dendrites were better resolved, showing them to consist of rows of multiple punctate junctions (**Figure 8A1**), and individual Cx36-puncta gathered in clusters along these dendrites (**Figure 8A2**) were seen nestled between and abutting the ends of multiple adherens junctions (**Figure 8A3**) that contacted the MAP2$^+$ dendrite (**Figure 8A4**).

To further assess association between Cx36-puncta and adherens junctions localized to dendrites at sites of mossy fiber terminals, high magnification single scan confocal images of labelling for Cx36 and nectin-1 in the stratum lucidum of rat ventral hippocampus were taken for immunofluorescence intensity profiling of labels for these proteins, with drawing of profiles oriented roughly perpendicular to the long axes of adherens junction strands, as shown in **Figure 9A**. Peak fluorescence intensities for labelling of Cx36 overlapped or fell within the margins of peak labelling intensities for nectin-1 (**Figure 9B**). Some Cx36-puncta in the field of **Figure 9A** show less overlap with nectin-1$^+$ labelling, which is likely due to the single scan approach to intensity profiling and which does

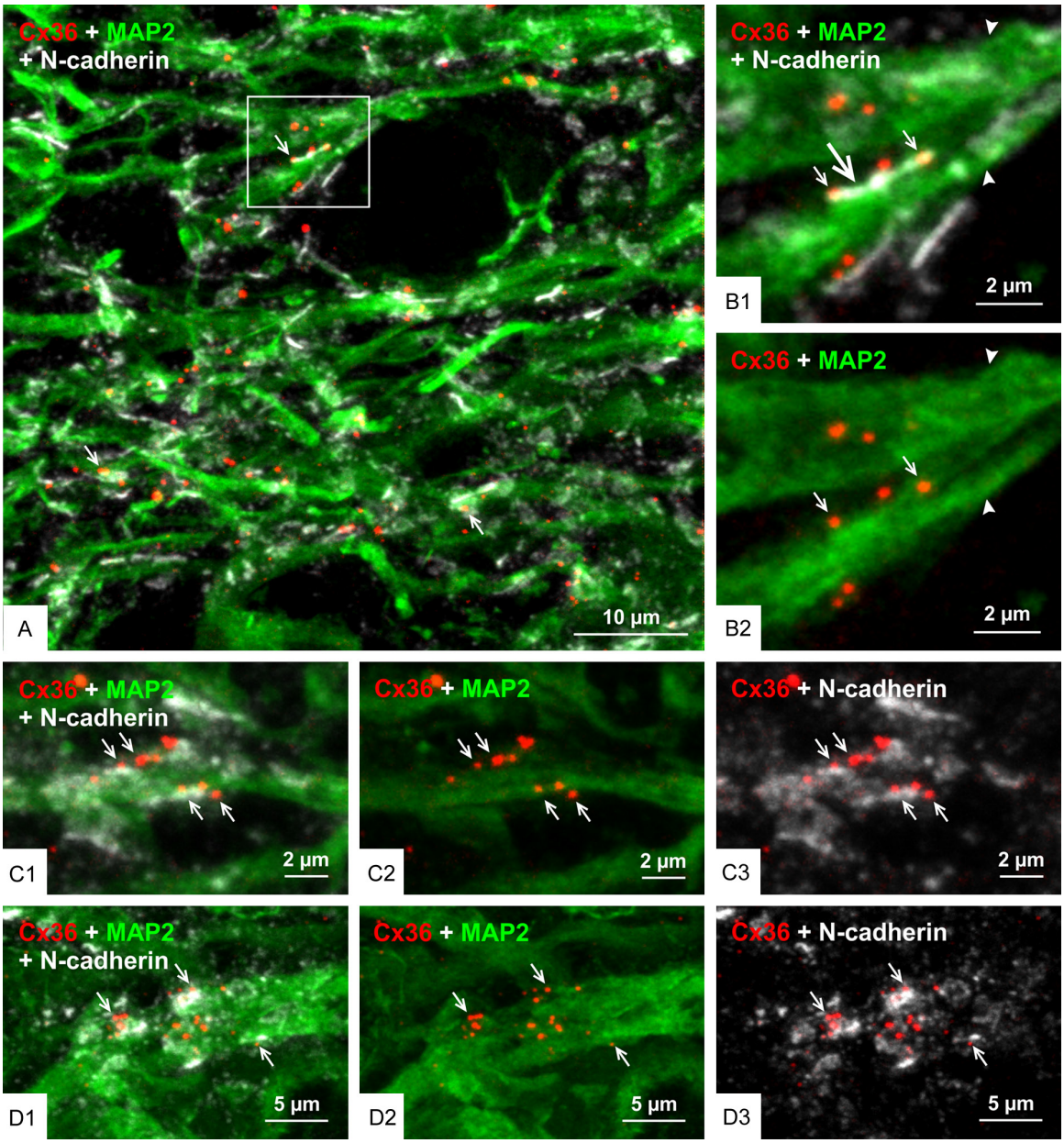

Figure 7. Configuration of Cx36-puncta and adherens junction in relation to CA3 pyramidal cell dendrites in the stratum lucidum of rat ventral hippocampus. (A) Triple immunofluorescence labelling in the CA3b region of the stratum lucidum showing numerous Cx36-puncta associated with N-cadherin$^+$ adherens junctions localized to CA3 pyramidal cell dendrites labelled for the microtubule marker MAP2 (arrows). (B) Higher magnification of the boxed area in (A), showing large MAP2$^+$ pyramidal cell dendrites (arrowheads) with a N-cadherin$^+$ adherens junction viewed on-edge along a dendrite (B1, large arrows) and several Cx36-puncta localized to the junction (B1, small arrows), where the Cx36-puncta are shown in red/green channel overlay (B2, arrows). (C) Triple labelling in the CA3c region of the stratum lucidum showing multiple Cx36-puncta co-distributed with N-cadherin$^+$ adherens junctions localized to both the upper and lower edges of a large MAP2$^+$ pyramidal cell dendrite (C1, arrows). The same image is shown with overlay of only the red/green channels and overlay of only the red/white channels to visualize Cx36-puncta association with the dendrite (C2, arrows) and with N-cadherin (C3, arrows). (D) Triple labelling in the CA3c stratum lucidum showing N-cadherin$^+$ adherens junctions viewed en-face and overlaying a MAP2$^+$ dendrite (D1, arrows), with clusters of Cx36-puncta (D2, arrows) closely associated with the adherens junctions that in en-face view appear to consist of multiple N-cadherin$^+$ puncta (D3, arrows).

not capture the full extent of the adherens junction. Because adherens junctions between mossy fiber terminals and CA3 pyramidal cells link these terminals directly to dendritic shafts

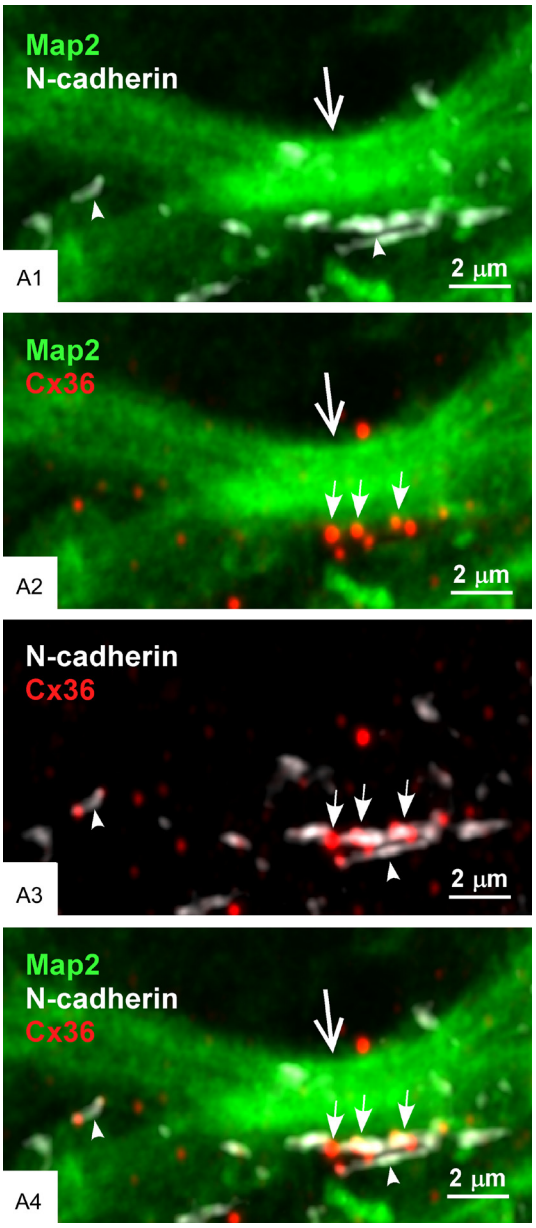

Figure 8. Higher resolution confocal airyscan imaging of the AJ-nGJ complex at CA3 pyramidal cell dendrites in stratum lucidum of rat ventral hippocampus. (A1-A4) Adherens junctions along MAP2$^+$ CA3 pyramidal cells dendrite (A1, large arrow) are shown to consist of multiple intermittent small junctions (A1, arrowheads), with the same region displaying a cluster of Cx36-puncta (A2, small arrows). Overlay of N-cadherin/Cx36 labelling shows Cx36-puncta abutted to the ends of individual junctional components of the N-cadherin$^+$ adherens junctions (A3, arrows), all of which is closely adjacent to the MAP2$^+$ CA3 pyramidal cell dendrite (A4).

[61, 65, 70, 71], the above results taken together suggest that Cx36-containing gap junctions also occur at terminal/shaft contacts, as depicted in **Figure 9C**.

The AJ-nGJ complex at mixed synapses in brainstem and spinal cord

To determine the generality with which Cx36 co-distributes with adherens junctions at mixed synapses, we examined several CNS locations in mouse and rat at which we have described Cx36-containing mixed synapses, including the lateral vestibular nucleus (LVN), the medial nucleus of the trapezoid body (MNTB), posteroventral cochlear nucleus (PVCN), ventral horn of the spinal cord and the red nucleus [51-53, 72]. In the LVN, the somata and proximal dendrites of large neurons are contacted by primary afferent terminals that form mixed synapses [72, 73]. A low magnification image of three such neurons (labelled with asterisks) is shown in **Figure 10A**, which is triple labelled for Cx36, N-cadherin and the additional marker zonula occluden-1 (ZO-1) that is a protein component of both nGJs and adherens junctions [26], thus providing confirmatory support for structural associations between these junctions. The LVN neurons are not counterstained, but a high density of immunolabelling for these three proteins delineated their soma and proximal dendrites. Higher confocal magnification of a single neuronal soma showed labelling of Cx36, N-cadherin and ZO-1 to be concentrated around the periphery of the soma in a typical punctate fashion (**Figure 10B1**, **10B2** and **10B3**, respectively). Total co-localization was seen between Cx36 and ZO-1 (**Figure 10B4**), as also seen in other brain regions [26], while labelling of N-cadherin together with either ZO-1 (**Figure 10B5**) or Cx36 (**Figure 10B6**) showed substantial overlap or were found in very close proximity. In the MNTB, large neuronal somata receive dense coverage and envelopment by calyx of Held terminals that originate from globular bushy cells in the anterior ventral cochlear nucleus. We previously reported that these calyciform terminals harbour Cx36-puncta, thus indicating the presence of Cx36-containing gap junctions at these terminals and their formation of mixed synapses on MNTB neuronal somata [52]. Labelling of Cx36 and N-cadherin on these somata showed that Cx36-puncta either partially overlapped with or were nestled immediately adjacent to punctate labelling of N-cadherin (**Figure 10C**, **10D**).

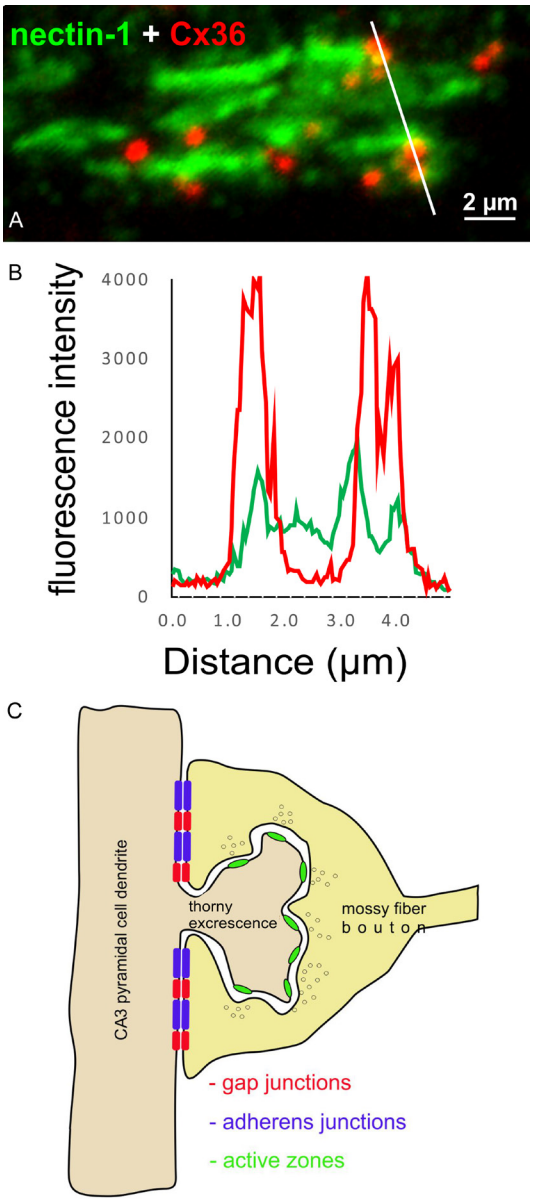

Figure 9. Immunofluorescence intensity profiling and loci of the AJ-nGJ complex at mossy fiber terminals on CA3 pyramidal cell dendrites. (A) Line profile of immunofluorescence labelling of Cx36 and nectin-1 at mossy fiber terminals in the ventral hippocampus of adult rat, with line tracking through several Cx36-puncta. (B) Histogram of immunofluorescence intensity along the white line in (A), showing overlap or close spatial proximity of peak labelling intensity for Cx36-puncta and nectin-1. (C) Schematic diagram illustrating locations of the components for mixed synaptic neurotransmission from mossy fiber terminals to CA3 pyramidal cell dendrites. The chemical synapse component is localized on the spine head at active zones and the electrical component consisting of Cx36-containing gap junctions closely associated with adherens junctions at the AJ-nGJ complex is localized at contacts between the mossy fiber terminal and dendritic shaft of the CA3 pyramidal cell.

However, N-cadherin puncta outnumbered Cx36-puncta, leaving some of those devoid of association with Cx36. Double labelling of these two proteins on large somata and dendrites in the PVCN showed their similar close association (**Figure 10E**) at what we previously described to be Cx36-containing mixed synapses [52]. In the lumbar spinal cord, it is well known that individual Ia muscle spindle afferents form multiple monosynaptic terminals on motoneurons throughout the motoneuron pools [74], and we have reported that these terminals form Cx36-containing mixed synapses [51]. Similarly, we have found that large neuronal somata in the brainstem red nucleus were laden with mixed synapses formed by nerve terminals of unknown origin [53]. Here, we show close association Cx36-puncta with N-cadherin at mixed synapses on both spinal cord motoneurons of adult rat (**Figure 11A**) and red nucleus neurons in adult mouse CNS (**Figure 11B**, **11C**). Thus, just as the AJ-nGJ complex is a widespread feature of purely electrical synapses [30], it appears that this complex is also a consistent structural component at mixed synapses.

Electrophysiological properties of mossy fiber-CA3 pathway in dorsal vs. ventral hippocampus

Given the presence of mixed synapses at mossy fiber terminals in the ventral but not dorsal hippocampus, we next examined whether any differences in frequency facilitation or LTP in the mossy fiber-CA3 pathway could be observed between these two regions. Slices from each hippocampal region were placed in a 6-well chamber with 2 to 3 slices per chamber. The first six and last six hippocampal slices (each 300 µm thick) taken along the rostrocaudal axis of the hippocampus were used for recording, which corresponded to the most dorsal or ventral portions of this structure, respectively. One of the characteristic properties of mossy fiber synapses is the frequency facilitation that these synapses undergo, where increasing the frequency of mossy fiber stimulation causes a pronounced increase in the field excitatory postsynaptic potential (fEPSP) recorded in the CA3 stratum lucidum. A minimum of 300% facilitation criteria was set for a recording to be included for the analysis and for determining the position of both recording and stimulating electrodes, as illustrated in **Figure**

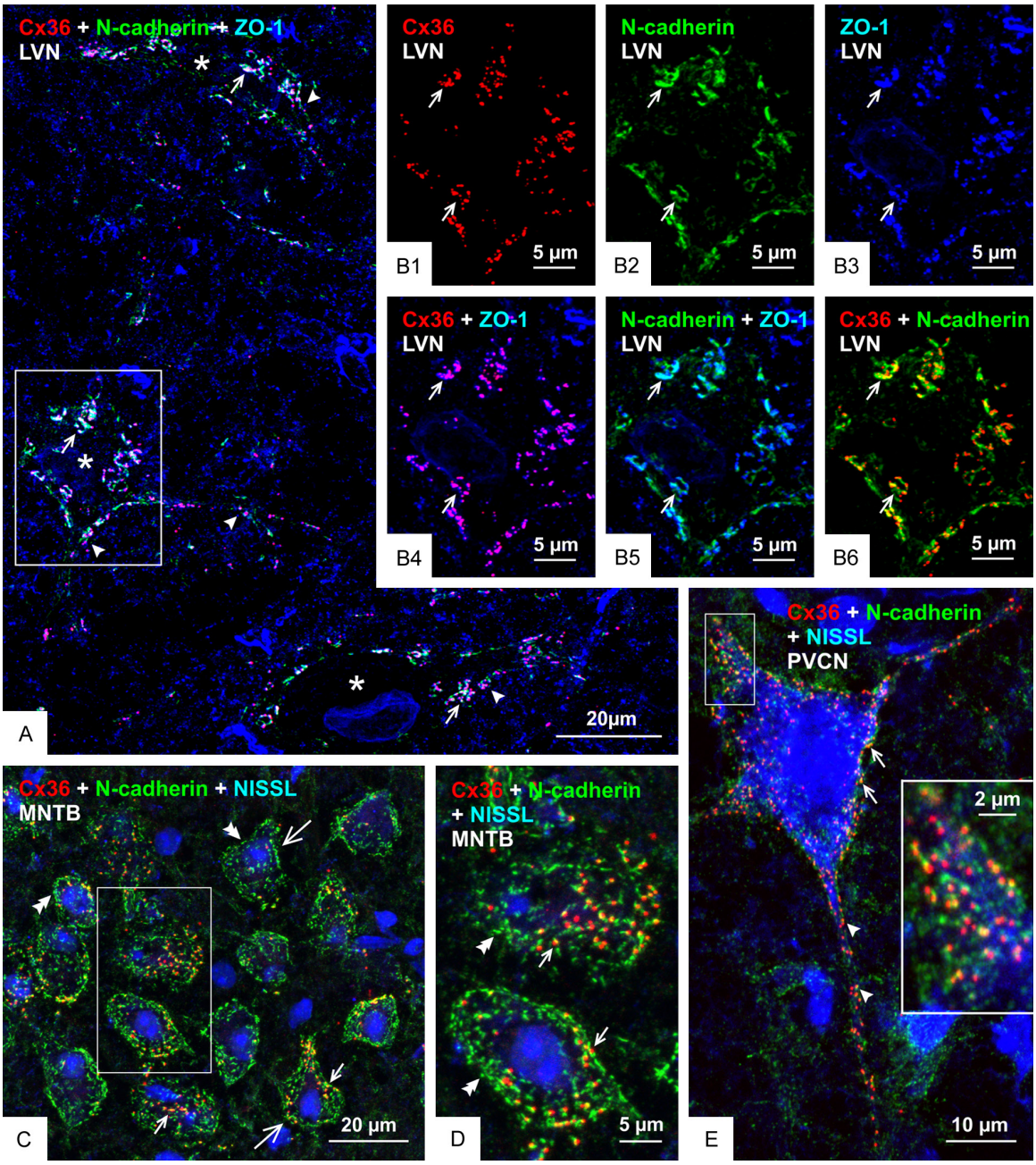

Figure 10. Relationships of Cx36, N-cadherin and ZO-1 at morphologically mixed synapses in the LVN, MNTB and PVCN of adult mouse. (A) Low magnification of the LVN, showing immunolabelling associated with three neuronal somata (not counterstained, but marked by asterisks) and their initial dendrites (arrowheads) decorated with Cx36-puncta that are co-localized with N-cadherin and ZO-1, seen as white in overlay of triple labelling (arrows). (B) Higher magnification of the boxed area at a neuronal somata in (A), showing individual labelling of Cx36-puncta (B1, arrows), N-cadherin (B2, arrows) and ZO-1 (B3, arrows), and with overlays showing near total co-localization of Cx36-puncta with ZO-1 (B4, arrows), substantial but not total co-localization of N-cadherin with ZO-1 (B5, arrows) and Cx36-puncta partially overlapping with or adjacent to labelling of N-cadherin (B6, arrows). (C, D) Overlay image of double labelling for Cx36 and N-cadherin with blue fluorescence counterstain in the MNTB, showing neuronal somata (C, large arrows; boxed area in C magnified in D) displaying Cx36-puncta associated with N-cadherin (small arrows) and patches of labelling for N-cadherin lacking association with Cx36-puncta (double arrowheads). (E) Overlay image showing Cx36-puncta association with N-cadherin on the somata (arrows) and initial dendrites (arrowheads) of a blue fluorescence counterstained octopus neuron in the PVCN, with the boxed area shown at higher magnification in the inset.

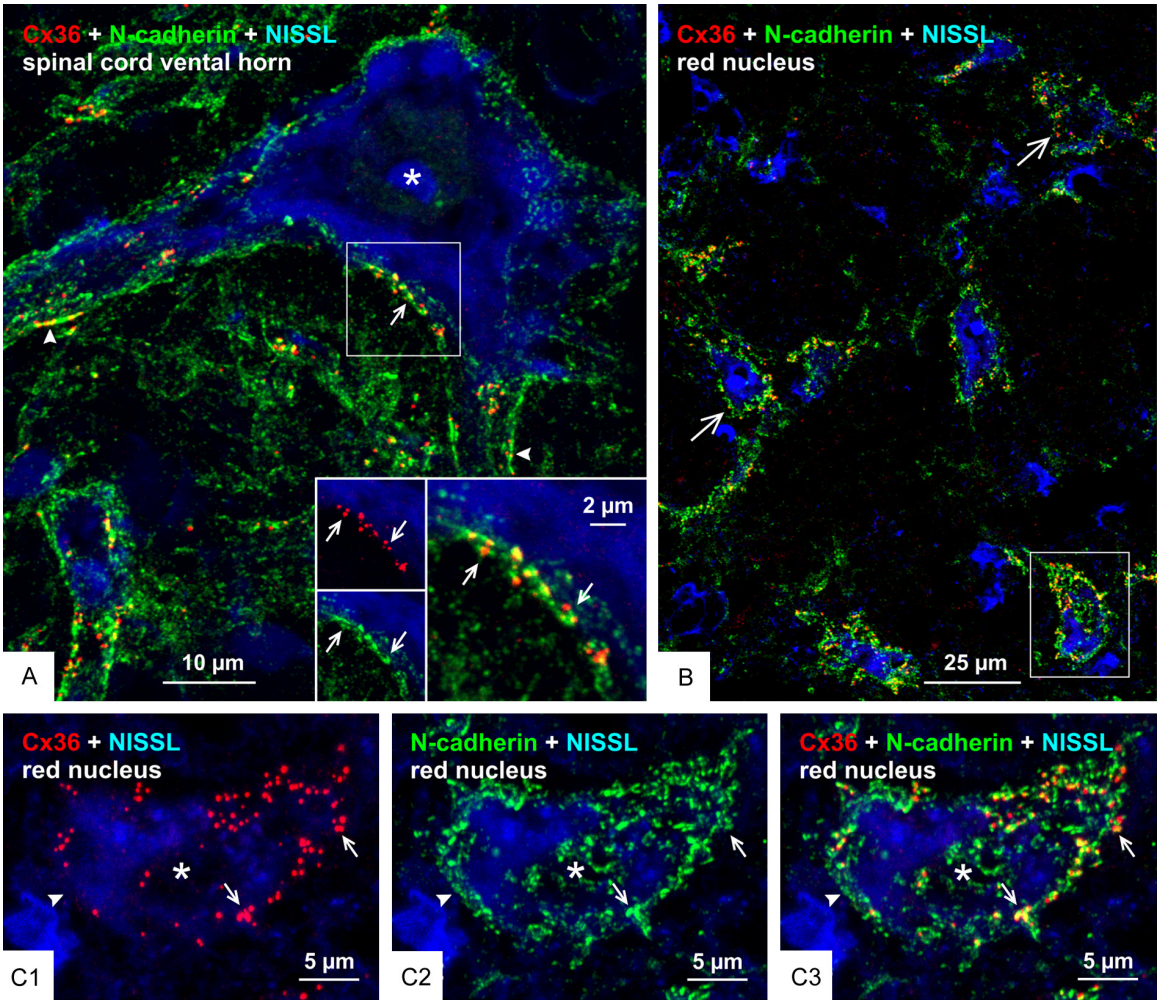

Figure 11. Relationships of Cx36 and N-cadherin at morphologically mixed synapses on motoneurons in the spinal cord and on large neurons in the red nucleus. (A) Double immunofluorescence labelling of Cx36 and N-cadherin with blue fluorescence Nissl counterstain in the lumbar spinal cord ventral horn of adult rat, showing overlay image of Cx36-puncta associated with labelling of N-cadherin on the somata (arrow) and initial dendrites (arrowheads) of a large motoneuron (asterisk), with inset of boxed area showing labelling of Cx36 (red) and N-cadherin (green) (arrows) shown magnified in overlay (arrow). (B) Double immunofluorescence labelling of Cx36 and N-cadherin with blue fluorescence Nissl counterstain in the red nucleus of adult mouse, with overlay image showing distribution of Cx36-puncta with N-cadherin on the surface of large neuronal somata (large arrows). (C) Magnification of the single neuronal somata (asterisk) in the boxed area of (B) (rotated clockwise by 90 degrees), showing nearly all somal Cx36-puncta (C1, arrows) associated with labelling of N-cadherin (C2, arrows), as seen in overlay (C3, arrows), and separate labelling of N-cadherin devoid of association with Cx36 (arrowhead).

12A. The percent increase in facilitation of mossy fiber fEPSP synaptic responses during mossy fiber stimulation was ~500% when recorded from 23 hippocampal slices obtained from 13 rats (**Figure 12B**). Frequency facilitation reflecting short-term plasticity was not significantly different between dorsal and ventral hippocampal slices (**Figure 12B**).

Next, we analyzed NMDA receptor (NMDAR) independent mossy fiber LTP [75] induced by high frequency stimulation (100 Hz for 1 sec, repeated twice at 20 sec intervals) in the presence of the NMDAR antagonist APV (50 µM). Subsequent to LTP induction, we find that potentiation was greater in ventral hippocampal slices (218 ± 24) compared with dorsal (160 ± 10, n=11; $P < 0.05$), unpaired t-test (**Figure 12C**), as further illustrated by comparing the potentiation 60 min after high-frequency stimulation in each region (**Figure 12D**). DCG-IV, applied at the end of LTP recordings,

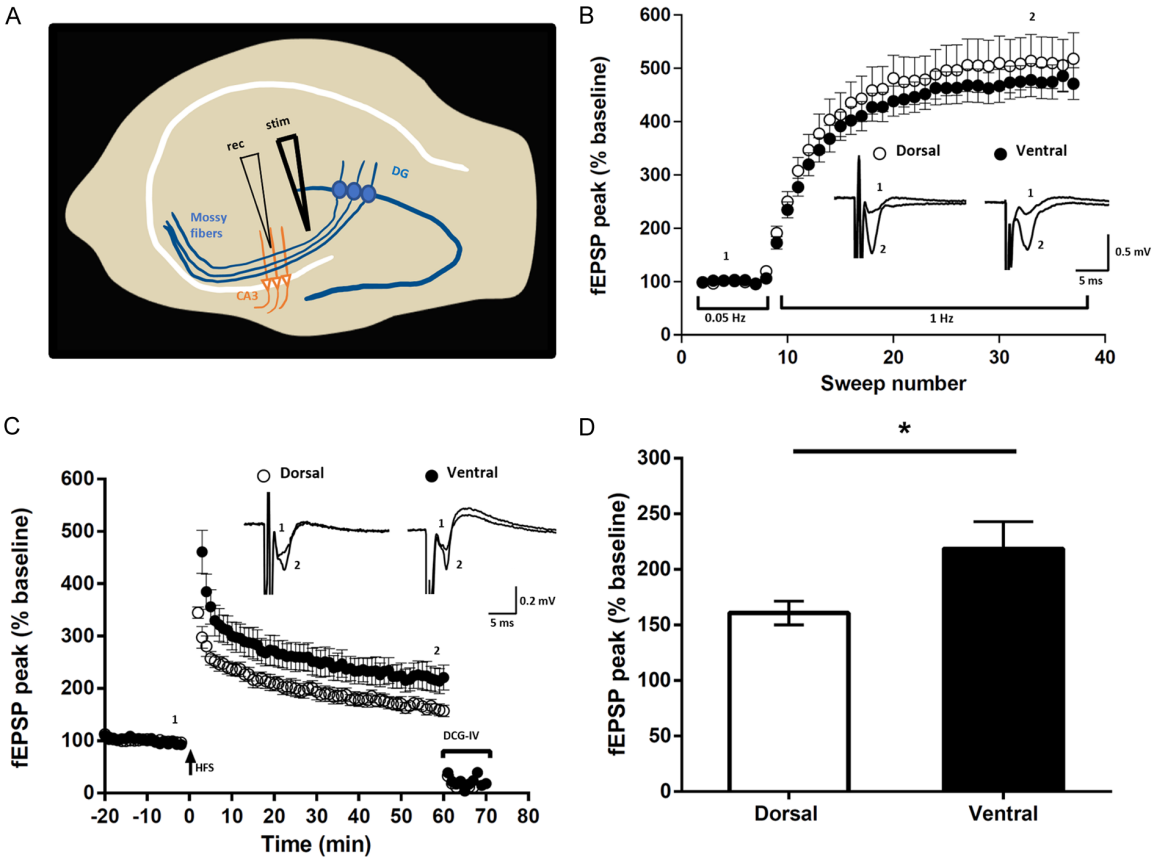

Figure 12. Properties of mossy fiber field EPSPs examined in transverse slices of rat dorsal vs. ventral hippocampus. A. Schematic of a hippocampal slice showing the positioning of stimulating (stim) and recording (rec) electrodes. B. Plot showing FF at mossy fiber synapses, where increased stimulation frequency from low (0.05 Hz) to moderate (1 Hz) stimulation produced a pronounced increase in fEPSP amplitude. Inset traces represent averaged response when stimulated at 0.05 Hz (1) and at 1 Hz (2) as indicated. C. Induction of LTP at mossy fiber synapses is independent of NMDAR activation, as shown by the persistence of mossy fiber LTP recorded in the presence of the NMDAR antagonist APV. Inset traces represent averaged response recorded before (1) and 60 min after high-frequency stimulation (HFS) (2) as indicated. At the end of the LTP induction protocol, the large degree of inhibition (75-80%) of fEPSPs by the mGluR2 agonist DCG-IV verified that stimulation evoked responses originated from activation of mossy fiber synapses. D. Averaged fEPSP amplitude measured from the last 5 min of LTP in dorsal and ventral hippocampal slices, showing significantly greater potentiation in the ventral slices. *P < 0.05, unpaired Student's t test with Welch's correction and error bars representing s.e.m.

reliably inhibited fEPSPs confirming that stimulation evoked responses originated from activation of mossy fiber synapses. Thus, our findings show that the magnitude of NMDAR-independent LTP at mossy fiber synapses is greater in ventral than in dorsal hippocampus.

Discussion

The present results extend our initial work demonstrating the association of Cx36-containing gap junctions with vglut1$^+$ mossy fiber terminals in the CA3b and CA3c subregions of the stratum lucidum in ventral hippocampus of adult rat [38]. In contrast to the localization of vglut1 in many different types of excitatory nerve terminals, the very high levels of vesicular ZnT3 in mossy fiber terminals [56, 57] afforded more specific immunofluorescence visualization of these structures and confirmed localization of multiple Cx36-puncta at a large percentage of those terminals in the above hippocampal subregions. These Cx36-puncta had a smaller range of sizes than those belonging to dendrites of parvalbumin$^+$ interneurons in the vicinity of the stratum lucidum, consistent with findings that ultrastructurally defined gap junctions examined by FRIL within this hippocampal layer generally had fewer connexon channels than

those linking dendrites of interneurons [40]. Although we found that most diminutive Cx36-puncta within the stratum lucidum were associated with $ZnT3^+$ mossy fiber terminals, some gap junctions of even smaller size have been identified by FRIL at various types of what were designated excitatory mixed synapses within this structure, including stratum lucidum. However, most of those as well as larger gap junctions could not be definitively identified to be associated specifically with mossy fiber terminals [40]. Based on thin-section EM approaches, putative gap junctional contacts between mossy fiber axons and at mossy fiber terminals have been reported [39, 40], but these failed to meet the heptalaminar criterion at plasma membrane contacts for designation as gap junctions. It is curious that bona fide gap junctional structures at mossy fiber terminals have not been reported despite extensive examination of these terminals by thin-section EM over the span of decades. However, it should be noted that exceptional ultrastructural preservation would be required to identify these structures. Further, much greater EM magnification would be required for their visualization than is typically used to observe chemical synaptic elements, particularly so given the very short lengths of gap junctions along neuronal plasma membranes.

Differential deployment of Cx36 at mossy fiber terminals vs. collaterals

In contrast to the occurrence of mixed synapses at mossy fiber terminals, our findings that the collaterals of these fibers forming filopodial extensions and *en passant* terminals lack Cx36-puncta and therefore fail to form mixed synapses raises four possibilities pertaining to how this can occur. First, it may be that only subpopulations of granule cells form mixed synapses at their mossy fiber terminals and these specifically lack collateral projections to the hilus and to mossy cells. This is unlikely based on quantitative analyses of the axonal ramifications of individual granule cells [62]. Second, Cx36 may be selectively transported to mossy fiber terminals, but not to mossy fiber collateral branches. This also is unlikely because it would require selectivity of protein transport at axonal branch points, where transport occurs along one branch but not another, for which we know of no precedent. Third, production of Cx36 protein from Cx36 mRNA may take place exclusively in mossy fiber terminals and mossy fiber collateral terminals may lack this capacity, however, this possibility suffers from the same problem as point two above. And fourth, as discussed below, adherens junctions may serve as structural determinants of subcellular sites at which nGJs are deployed. This possibility is supported by the formation of numerous adherens junctions by mossy fiber terminals and the absence of these junctions between the postsynaptic targets of filopodial extensions or *en passant* terminals [62]. Cx36 may be transported along mossy fiber axon collaterals, but it may be rapidly recirculated in the absence of molecular machinery for its incorporation into gap junctions within the plasma membrane.

It is interesting to consider this mixed synaptic feature that distinguishes the terminal types of mossy fibers in the context of Dale's principle [76], which as reformulated by Eccles et al. [77] states "In conformity with Dale's principle that the same chemical transmitter is released from all the synaptic terminals of a neuron …". Although this principle applies to chemical synaptic transmission and was formulated before electrical synapses were identified, it seems reasonable to consider that all terminals of a neuron should have that same transmission capabilities regardless of the nature of that transmission (i.e., chemical or electrical). If this is a legitimate tenet, then it would appear that the electrical component of mixed synapses violates Dale's principle, at least in the case of hippocampal granule cells and their projections.

The AJ-nGJ complex at mixed synapses

Adherens junctions and gap junctions composed of various connexins have intimate structural and functional interactions in peripheral tissues [78], where it has been established that cell adhesion mediated via N-cadherin or E-cadherin is required for the formation of gap junctions [79-83]. Similarly, nGJs were frequently noted to be in structural continuity with adherens junctions in a variety of brain regions [84-89] and we have found that the AJ-nGJ complex is a general feature of purely electrical synapses formed between many types of neurons [30]. Adherens junctions independent of nGJs also link a wide variety of neuronal subcel-

lular elements, including nerve terminals to their postsynaptic elements [90-92]. Here, we show that the AJ-nGJ complex is also prominent at mixed synapses that have been identified in the mammalian CNS. Among the best characterized adherens junctions (aka, puncta adherentia) are those joining large mossy fiber terminals exclusively to the dendritic shafts of CA3 pyramidal cells in the stratum lucidum of the hippocampus, where these junctions consist of a series of multiple (ranging from 2-13), closely spaced contacts per terminal [61, 65, 70, 71]. The protein constituents of these junctions, including N-cadherin, nectins and ZO-1, have been extensively studied and their visualization by immunofluorescence shows the series of contacts they form to be merged as distinctive linear strands [66, 93-96]. This is of note because it could then be presumed that the Cx36-puncta we observe associated with adherens junctions at mixed synapses represent gap junctions interdigitated between and among these intermittently localized and closely spaced adherens junctions, which was evident here in some on-edge and en-face views of the AJ-nGJ complex. This is consistent with the reported close proximity between adherens junctions and gap junctions at some mixed synapses examined ultrastructurally in other regions of mammalian brain [97].

In addition to N-cadherin, nectins and ZO-1, other key proteins found at adherens junctions of mossy fiber terminals include AF6 (aka, afadin), α-catenin and β-catenin [38, 66, 68, 93, 94], all of which are also found in close association with nGJs at purely electrical synapses [30]. Based on an assortment of known direct molecular interactions between these proteins, we have previously proposed a model whereby these interactions may physically tether nGJs to adjacent adherens junctions at these synapses [30]. Specifically, it is known that nectin-1 interacts with AF6 linked to ZO-1, that cadherins bind α-catenin and β-catenin, and that the nectin-AF6 and cadherin-catenin systems associate through AF6-α-catenin interaction [98, 99] to co-operatively organize adherens junctions [100-103]. The reported association of ZO-1 and AF6 with both adherens junctions and nGJs [26, 27, 104-106], together with the known direct molecular interaction of the carboxy-terminus motif of Cx36 with PDZ (PSD-95, DlgA, ZO-1) domains contained in each of ZO-1 and AF6, provide a mechanism for molecular links involving AF6/ZO-1/Cx36 and/or AF6/Cx36 interactions between these two types of intercellular junctions [30]. The present results suggest that a similar set of molecular interactions mediate tethering of nGJ to adherens junctions at the AJ-nGJ complex now identified at mixed synapses. More broadly, our studies of the AJ-nGJ complex in Cx36 null mice [30] suggest that various components of this AJ-nGJ complex serve as pre-existing nucleation sites for assembly of Cx36-containing gap junctions, which is consistent with targeting of other connexins to adherens junctions in various cell types [80, 107], and this may also occur at mixed synapses.

Loci and functional consequence of the AJ-nGJ complex at mossy fiber terminals

The presence of the AJ-nGJ complex at mossy fiber terminals, together with the known localization of adherens junctions exclusively at plasma membrane of these terminals that contact the dendritic shafts of CA3 pyramidal cells [61, 65, 70, 71], strongly suggest that gap junctions are highly restricted to compartments directly linking mossy fiber terminals to dendritic shafts (**Figure 9**). In contrast, chemical transmission at these terminals occurs at active zones distributed around thorny excrescences emanating from CA3 pyramidal cell dendrites, but not at direct terminal-dendritic shaft contacts where there is a paucity of synaptic vesicles and an absence of active zones (ibid, above). It thus appears that mossy fiber terminals exhibit spatial separation of subcellular loci that mediate the chemical *vs.* electrical components of their mixed synaptic transmission. This configuration could have several important consequences for functional interactions between the two forms of communication and thus properties imparted onto mixed mossy fiber synapses on CA3 pyramidal cells [108]. First, the electrical component could produce subthreshold dendritic depolarizations that summate with the chemical transmission component at spines to facilitate dendrite activation. Second, pyramidal cell spike or burst activity could be propagated antidromically via the electrical component into multiple spine heads to enhance chemical synaptic activation of spines. Third, electrical synapses at mossy fiber terminals may participate in transmission

of signals that arrive to these terminals in an analog fashion, where varying magnitudes of subthreshold depolarizations below the level to generate action potentials in granule cells are propagated along mossy fibers, creating subthreshold depolarizations of mossy fiber terminals [109]. The low pass filtering properties of nGJs would be ideal for transmitting these low amplitude and relatively long duration depolarization to the dendritic shafts of postsynaptic CA3 pyramidal cells, perhaps priming those dendrites for further mossy fiber input. And fourth, at neuronal microcompartments such as the dendritic spine head/neck assembly, electrical field effects have been considered to have an impact on electrical current flow between this assembly and the dendritic shaft following synaptic activation of spine heads [110]. We speculate that the strategic placement of gap junctional channels could influence those field effects by modulating the voltage drop between spine head and dendritic shaft, which may serve to modify synaptic transmission efficacy.

Conclusion: mossy fiber terminals in ventral vs. dorsal hippocampus

The highly restricted distribution of mixed synapses and the unique properties bestowed by the mixed electrical/chemical mode of transmission suggests that they impart highly specialized functions to circuits in which they occur. Of note, within cortical and neocortical structures, Cx36-containing mixed synapses are only found within the ventral (but not the dorsal) hippocampus and are uniquely present at mossy fiber terminals forming giant synapses (3-6 μm diameter) upon dendrites of CA3 pyramidal neurons. Giant mossy fiber terminals, in both ventral and dorsal hippocampus, are recognized as conditional detonators, able to elicit postsynaptic firing with high fidelity during repetitive activity [111, 112]. While the dorsal hippocampus is associated with navigation, exploration and locomotion, and supports spatial learning and memory, the ventral hippocampus, heavily connected to the hypothalamus, amygdala and prefrontal cortex, serves memory functions related to motivational, emotional and affective states [113]. Given such functional segmentation along the rostral/caudal hippocampal axis, the finding of substantial differences in LTP magnitude, as we have observed and as previously reported by others [114-116], is not unexpected. Such differences have been more widely recognized within the hippocampal CA1 region where reports demonstrate a greater propensity for LTP in dorsal compared with the ventral hippocampus [114, 115]. Fewer studies have characterized dorsoventral differences in the dentate gyrus. Our findings, demonstrating enhanced LTP at mossy fiber terminals in CA3 of ventral hippocampus, therefore lend support to functional segmentation along the dorsoventral hippocampal axis and within hippocampal subregions. Several mechanisms could underly the dorsal vs. ventral difference we observe, including change in excitation/inhibition balance [116], which will require further study. However, given the known reliable nature of direct electrical transmission at purely electrical synapses, the additional presence of electrical synapses at giant mossy terminals may serve as a means for ensuring absolute transmission fidelity at this critical relay. In this manner, we speculate that these synapses can function as a strategic element in hippocampal synaptic circuitry to guarantee efficient storage and recall of aversive memories during distressful events such as those evoking fear. Our findings that mixed synapses occur not only in rat but also in human ventral hippocampus underscores the potential role of these synapses in governing neural communication underlying encoding and retrieval of emotional memory in hippocampal circuitry. This may have important consequences for understanding not only the physiological basis of important higher cognitive functions, but also neuropsychiatric disorders such as depression, anxiety, and post-traumatic stress disorder where disordered function of ventral hippocampus has been implicated.

Acknowledgements

This work was supported by grants from the Canadian Institutes of Health Research, the Canadian Natural Sciences and Engineering Research Council to J.I.N. and M.F.J., and the University of Manitoba Rady Innovation Fund to J.I.N. and M.F.J. We thank B. McLean and P. Silwal for excellent technical assistance.

Disclosure of conflict of interest

None.

Abbreviations

aCSF, artificial cerebrospinal fluid; AJ-nGJ, adherens junction-neuronal gap junction complex; CNS, central nervous system; Cx36, connexin36; DCG-IV, dicarboxycyclopropyl glycine; E-cadherin, epithelial cadherin; fEPSP, field excitatory postsynaptic potential; FF, frequency facilitation; FRIL, freeze-fracture replica immunogold labelling; HFS, high-frequency stimulation; LTP, long term potentiation; LVN, lateral vestibular nucleus; MAP2, microtubule-associated protein2; MF, mossy fiber; MNTB, medial nucleus of the trapezoid body; N-cadherin, neural cadherin; nGJs, neuronal gap junctions; NMDG, N-Methyl-D-glucamine; PBS, phosphate buffer containing 0.9% saline; PDZ, PSD-95, DlgA, ZO-1 domains; PVCN, posteroventral cochlear nucleus; TBS, 50 mM Tris-HCl containing 1.5% sodium chloride; TBST, 50 mM Tris-HCl containing 1.5% sodium chloride and 0.3% Triton X-100; Vglut1, vesicular glutamate transporter1; ZnT3, vesicular zinc transporter-3; ZO-1, zonula occludens-1.

Address correspondence to: Dr. James I Nagy, Department of Physiology and Pathophysiology, Rady Faculty of Health Sciences, Max Rady College of Medicine, University of Manitoba, 745 Bannatyne Avenue, Winnipeg, Manitoba R3E 0J9, Canada. Tel: 204-789-3767; Fax: 204-789-3934; E-mail: James.Nagy@umanitoba.ca

References

[1] Connors BW and Long MA. Electrical synapses in the mammalian brain. Annu Rev Neurosci 2004; 27: 393-418.

[2] Connors BW. Electrical signaling with neuronal gap junctions. In: Harris A, Locke D, editors. Connexins: A Guide. Springer: Humana Press; 2009. pp. 143-164.

[3] Pereda AE, Curti S, Hoge G, Cachope R, Flores CE and Rash JE. Gap junction-mediated electrical transmission: regulatory mechanisms and plasticity. Biochim Biophys Acta 2013; 1828: 134-146.

[4] Pereda AE. Electrical synapses and their functional interactions with chemical synapses. Nat Rev Neurosci 2014; 15: 250-263.

[5] Nagy JI, Pereda AE and Rash JE. Electrical synapses in mammalian CNS: past eras, present focus and future directions. Biochim Biophys Acta Biomembr 2018; 1860: 102-123.

[6] Alcami P and Pereda AE. Beyond plasticity: the dynamic impact of electrical synapses on neural circuits. Nat Rev Neurosci 2019; 20: 253-271.

[7] Evans WH and Martin PE. Gap junctions: structure and function (review). Mol Membr Biol 2002; 19: 121-136.

[8] Goodenough DA and Paul DL. Gap junctions. Cold Spring Harb Perspect Biol 2009; 1: a002576.

[9] Bennett MV. Gap junctions as electrical synapses. J Neurocytol 1997; 26: 349-366.

[10] Condorelli DF, Belluardo N, Trovato-Salinaro A and Mudo G. Expression of Cx36 in mammalian neurons. Brain Res Brain Res Rev 2000; 32: 72-85.

[11] Condorelli DF, Trovato-Salinaro A, Mudò G, Mirone MB and Belluardo N. Cellular expression of connexins in the rat brain: neuronal localization, effects of kainate-induced seizures and expression in apoptotic neuronal cells. Eur J Neurosci 2003; 18: 1807-1827.

[12] Rash JE, Staines WA, Yasumura T, Patel D, Furman CS, Stelmack GL and Nagy JI. Immunogold evidence that neuronal gap junctions in adult rat brain and spinal cord contain connexin-36 but not Cx32 or Cx43. Proc Natl Acad Sci U S A 2000; 97: 7573-7578.

[13] Rash JE, Yasumura T, Dudek FE and Nagy JI. Cell-specific expression of connexins and evidence of restricted gap junctional coupling between glial cells and between neurons. J Neurosci 2001; 21: 1983-2000.

[14] Rash JE, Pereda A, Kamasawa N, Furman CS, Yasumura T, Davidson KG, Dudek FE, Olson C, Li X and Nagy JI. High-resolution proteomic mapping in the vertebrate central nervous system: close proximity of connexin35 to NMDA glutamate receptor clusters and co-localization of connexin36 with immunoreactivity for zonula occludens protein-1 (ZO-1). J Neurocytol 2004; 33: 131-151.

[15] Rash JE, Olson CO, Pouliot WA, Davidson KG, Yasumura T, Furman CS, Royer S, Kamasawa N, Nagy JI and Dudek FE. Connexin36 vs. connexin32, "miniature" neuronal gap junctions, and limited electrotonic coupling in rodent suprachiasmatic nucleus. Neuroscience 2007; 149: 350-371.

[16] Rash JE, Olson CO, Davidson KG, Yasumura T, Kamasawa N and Nagy JI. Identification of connexin36 in gap junctions between neurons in rodent locus coeruleus. Neuroscience 2007; 147: 938-956.

[17] Nagy JI, Dudek FE and Rash JE. Update on connexins and gap junctions in neurons and glia in the mammalian nervous system. Brain Res Brain Res Rev 2004; 47: 191-215.

[18] Bennett MV and Zukin RS. Electrical coupling and neuronal synchronization in the mammalian brain. Neuron 2004; 41: 495-511.

[19] Hormuzdi SG, Filippov MA, Mitropoulou G, Monyer H and Bruzzone R. Electrical synapses: a dynamic signaling system that shapes the activity of neuronal networks. Biochim Biophys Acta 2004; 1662: 113-137.
[20] Haas JS, Zavala B and Landisman CE. Activity-dependent long-term depression of electrical synapses. Science 2011; 334: 389-393.
[21] Haas JS and Landisman CE. Bursts modify electrical synaptic strength. Brain Res 2012; 1487: 140-149.
[22] Mathy A, Clark BA and Hausser M. Synaptically induced long-term modulation of electrical coupling in the inferior olive. Neuron 2014; 81: 1290-1296.
[23] Turecek J, Yuen GS, Han VZ, Zeng XH, Bayer KU and Welsh JP. NMDA receptor activation strengthens weak electrical coupling in mammalian brain. Neuron 2014; 81: 1375-1388.
[24] O'Brien J. The ever-changing electrical synapse. Curr Opin Neurobiol 2014; 29: 64-72.
[25] O'Brien J. Design principles of electrical synaptic plasticity. Neurosci Lett 2019; 695: 4-11.
[26] Li X, Olson C, Lu S, Kamasawa N, Yasumura T, Rash JE and Nagy JI. Neuronal connexin36 association with zonula occludens-1 protein (ZO-1) in mouse brain and interaction with the first PDZ domain of ZO-1. Eur J Neurosci 2004; 19: 2132-2146.
[27] Li X, Lynn BD and Nagy JI. The effector and scaffolding proteins AF6 and MUPP1 interact with connexin36 and localize at gap junctions that form electrical synapses in rodent brain. Eur J Neurosci 2012; 35: 166-181.
[28] Lynn BD, Li X and Nagy JI. Under construction: building the macromolecular superstructure and signaling components of an electrical synapse. J Membr Biol 2012; 245: 303-317.
[29] Lynn BD, Li X, Hormuzdi SG, Griffiths EK, McGlade CJ and Nagy JI. E3 ubiquitin ligases LNX1 and LNX2 localize at neuronal gap junctions formed by connexin36 in rodent brain and molecularly interact with connexin36. Eur J Neurosci 2018; 48: 3062-3081.
[30] Nagy JI and Lynn BD. Structural and intermolecular associations between connexin36 and protein components of the adherens junction-neuronal gap junction complex. Neuroscience 2018; 384: 241-261.
[31] Hormuzdi SG, Pais I, LeBeau FE, Towers SK, Rozov A, Buhl EH, Whittington MA and Monyer H. Impaired electrical signaling disrupts gamma frequency oscillations in connexin 36-deficient mice. Neuron 2001; 31: 487-495.
[32] Kosaka T and Hama K. Gap junctions between non-pyramidal cell dendrites in the rat hippocampus (CA1 and CA3 regions): a combined Golgi-electron microscopy study. J Comp Neurol 1985; 231: 150-161.
[33] Posluszny A. The contribution of electrical synapses to field potential oscillations in the hippocampal formation. Front Neural Circuits 2014; 8: 32.
[34] Dudek F, Andrew RD, MacVicar BA, Snow RW and Taylor CP. Recent evidence for and possible significance of gap junctions and electrotonic synapses in the mammalian brain. In: Jasper HH, van Gelder NM, editors. Basic Mechanisms of Neuronal Hyperexcitability. New York: Alan R Liss; 1983. pp. 31-73.
[35] Mercer A, Bannister AP and Thomson AM. Electrical coupling between pyramidal cells in adult cortical regions. Brain Cell Biol 2006; 35: 13-27.
[36] Schmitz D, Schuchmann S, Fisahn A, Draguhn A, Buhl EH, Petrasch-Parwez E, Dermietzel R, Heinemann U and Traub RD. Axo-axonal coupling. A novel mechanism for ultrafast neuronal communication. Neuron 2001; 31: 831-840.
[37] Traub RD and Whittington MA. Cortical Oscillations in Health and Disease. New York: Oxford University Press; 2010.
[38] Nagy JI. Evidence for connexin36 localization at hippocampal mossy fiber terminals suggesting mixed chemical/electrical transmission by granule cells. Brain Res 2012; 1487: 107-122.
[39] Hamzei-Sichani F, Kamasawa N, Janssen WG, Yasumura T, Davidson KG, Hof PR, Wearne SL, Stewart MG, Young SR, Whittington MA, Rash JE and Traub RD. Gap junctions on hippocampal mossy fiber axons demonstrated by thin-section electron microscopy and freeze fracture replica immunogold labeling. Proc Natl Acad Sci U S A 2007; 104: 12548-12553.
[40] Hamzei-Sichani F, Davidson KG, Yasumura T, Janssen WG, Wearne SL, Hof PR, Traub RD, Gutierrez R, Ottersen OP and Rash JE. Mixed electrical-chemical synapses in adult rat hippocampus are primarily glutamatergic and coupled by connexin-36. Front Neuroanat 2012; 6: 13.
[41] Vivar C, Traub RD and Gutiérrez R. Mixed electrical-chemical transmission between hippocampal mossy fibers and pyramidal cells. Eur J Neurosci 2012; 35: 76-82.
[42] Ixmatlahua DJ, Vizcarra B, Gómez-Lira G, Romero-Maldonado I, Ortiz F, Rojas-Piloni G and Gutiérrez R. Neuronal glutamatergic network electrically wired with silent but activatable gap junctions. J Neurosci 2020; 40: 4661-4672.
[43] Gutierrez R. Gap junctions in the brain: hardwired but functionally versatile. Neuroscientist 2023; 29: 554-568.
[44] Curti S, Hoge G, Nagy JI and Pereda AE. Synergy between electrical coupling and membrane properties promotes strong synchronization of

neurons of the mesencephalic trigeminal nucleus. J Neurosci 2012; 32: 4341-4359.
[45] Xie YF, Belrose JC, Lei G, Tymianski M, Mori Y, MacDonald JF and Jackson MF. Dependence of NMDA/GSK-3β mediated metaplasticity on TRPM2 channels at hippocampal CA3-CA1 synapses. Mol Brain 2011; 4: 44.
[46] Yang K, Trepanier C, Sidhu B, Xie YF, Li H, Lei G, Salter MW, Orser BA, Nakazawa T, Yamamoto T, Jackson MF and MacDonald JF. Metaplasticity gated through differential regulation of GluN2A versus GluN2B receptors by Src family kinases. EMBO J 2012; 31: 805-816.
[47] Yang K, Lei G, Xie YF, MacDonald JF and Jackson MF. Differential regulation of NMDAR and NMDAR-mediated metaplasticity by anandamide and 2-AG in the hippocampus. Hippocampus 2014; 24: 1601-1614.
[48] Sun HS, Jackson MF, Martin LJ, Jansen K, Teves L, Cui H, Kiyonaka S, Mori Y, Jones M, Forder JP, Golde TE, Orser BA, MacDonald JF and Tymianski M. Suppression of hippocampal TRPM7 protein prevents delayed neuronal death in brain ischemia. Nat Neurosci 2009; 12: 1300-1307.
[49] Kamasawa N, Furman CS, Davidson KG, Sampson JA, Magnie AR, Gebhardt BR, Kamasawa M, Yasumura T, Zumbrunnen JR, Pickard GE, Nagy JI and Rash JE. Abundance and ultrastructural diversity of neuronal gap junctions in the OFF and ON sublaminae of the inner plexiform layer of rat and mouse retina. Neuroscience 2006; 142: 1093-1117.
[50] Bautista W and Nagy JI. Connexin36 in gap junctions forming electrical synapses between motoneurons in sexually dimorphic motor nuclei in spinal cord of rat and mouse. Eur J Neurosci 2014; 39: 771-787.
[51] Bautista W, McCrea DA and Nagy JI. Connexin36 identified at morphologically mixed chemical/electrical synapses on trigeminal motoneurons and at primary afferent terminals on spinal cord neurons in adult mouse and rat. Neuroscience 2014; 263: 159-180.
[52] Rubio ME and Nagy JI. Connexin36 expression in major centers of the auditory system in the CNS of mouse and rat: evidence for neurons forming purely electrical synapses and morphologically mixed synapses. Neuroscience 2015; 303: 604-629.
[53] Nagy JI, Pereda AE and Rash JE. On the occurrence and enigmatic functions of mixed (chemical plus electrical) synapses in the mammalian CNS. Neurosci Lett 2019; 695: 53-64.
[54] Fukuda T. Network architecture of gap junction-coupled neuronal linkage in the striatum. J Neurosci 2009; 29: 1235-1243.
[55] Shigematsu N, Nishi A and Fukuda T. Gap junctions interconnect different subtypes of parvalbumin-positive interneurons in barrels and septa with connectivity unique to each subtype. Cereb Cortex 2019; 29: 1414-1429.
[56] Palmiter RD, Cole TB, Quaife CJ and Findley SD. ZnT-3, a putative transporter of zinc into synaptic vesicles. Proc Natl Acad Sci U S A 1996; 93: 14934-14939.
[57] Wenzel HJ, Cole TB, Born DE, Schwartzkroin PA and Palmiter RD. Ultrastructural localization of zinc transporter-3 (ZnT-3) to synaptic vesicle membranes within mossy fiber boutons in the hippocampus of mouse and monkey. Proc Natl Acad Sci U S A 1997; 94: 12676-12681.
[58] Scharfman HE. Spiny neurons of area CA3c in rat hippocampal slices have similar electrophysiological characteristics and synaptic responses despite morphological variation. Hippocampus 1993; 3: 9-28.
[59] Ishizuka N, Cowan WM and Amaral DG. A quantitative analysis of the dendritic organization of pyramidal cells in the rat hippocampus. J Comp Neurol 1995; 362: 17-45.
[60] Ramon y Cajal S. Histologie de systeme nerveux de l'homme et des vertebres tomme II. Paris: Maloine; 1911.
[61] Amaral DG. Synaptic extensions from the mossy fibers of the fascia dentata. Anat Embryol (Berl) 1979; 155: 241-251.
[62] Acsady L, Kamondi A, Sik A, Freund T and Buzsaki G. GABAergic cells are the major postsynaptic targets of mossy fibers in the rat hippocampus. J Neurosci 1998; 18: 3386-3403.
[63] Scharfman HE, Kunkel DD and Schwartzkroin PA. Synaptic connections of dentate granule cells and hilar neurons: results of paired intracellular recordings and intracellular horseradish peroxidase injections. Neuroscience 1990; 37: 693-707.
[64] Amaral DG. A Golgi study of cell types in the hilar region of the hippocampus in the rat. J Comp Neurol 1978; 182: 851-914.
[65] Chicurel ME and Harris KM. Three-dimensional analysis of the structure and composition of CA3 branched dendritic spines and their synaptic relationships with mossy fiber boutons in the rat hippocampus. J Comp Neurol 1992; 325: 169-82.
[66] Inagaki M, Irie K, Deguchi-Tawarada M, Ikeda W, Ohtsuka T, Takeuchi M and Takai Y. Nectin-dependent localization of ZO-1 at puncta adhaerentia junctions between the mossy fiber terminals and the dendrites of the pyramidal cells in the CA3 area of adult mouse hippocampus. J Comp Neurol 2003; 460: 514-524.
[67] Irie K, Shimizu K, Sakisaka T, Ikeda W and Takai Y. Roles and modes of action of nectins

in cell-cell adhesion. Semin Cell Dev Biol 2004; 15: 643-656.
[68] Majima T, Ogita H, Yamada T, Amano H, Togashi H, Sakisaka T, Tanaka-Okamoto M, Ishizaki H, Miyoshi J and Takai Y. Involvement of afadin in the formation and remodeling of synapses in the hippocampus. Biochem Biophys Res Commun 2009; 385: 539-544.
[69] Pivovarova NB, Pozzo-Miller LD, Hongpaisan J and Andrews SB. Correlated calcium uptake and release by mitochondria and endoplasmic reticulum of CA3 hippocampal dendrites after afferent synaptic stimulation. J Neurosci 2002; 22: 10653-10661.
[70] Amaral DG and Dent JA. Development of the mossy fibers of the dentate gyrus: I. A light and electron microscopic study of the mossy fibers and their expansions. J Comp Neurol 1981; 195: 51-86.
[71] Rollenhagen A, Satzler K, Rodriguez EP, Jonas P, Frotscher M and Lubke JH. Structural determinants of transmission at large hippocampal mossy fiber synapses. J Neurosci 2007; 27: 10434-10444.
[72] Nagy JI, Bautista W, Blakley B and Rash JE. Morphologically mixed chemical-electrical synapses formed by primary afferents in rodent vestibular nuclei as revealed by immunofluorescence detection of connexin36 and vesicular glutamate transporter-1. Neuroscience 2013; 252: 468-488.
[73] Korn H, Sotelo C and Crepel F. Electronic coupling between neurons in the rat lateral vestibular nucleus. Exp Brain Res 1973; 16: 255-275.
[74] Brown AG and Fyffe RE. The morphology of group Ia afferent fibre collaterals in the spinal cord of the cat. J Physiol 1978; 274: 111-127.
[75] Zalutsky RA and Nicoll RA. Comparison of two forms of long-term potentiation in single hippocampal neurons. Science 1990; 248: 1619-1624.
[76] Dale HH. Pharmacology and nerve-ending. Proc R Soc Med 1934; 28: 319-30.
[77] Eccles JC, Fatt P and Koketsu K. Cholinergic and inhibitory synapses in a pathway from motor-axon collaterals to motoneurons. J Physiol 1954; 126: 524-62.
[78] Derangeon M, Spray DC, Bourmeyster N, Sarrouilhe D and Herve JC. Reciprocal influence of connexins and apical junction proteins on their expressions and functions. Biochim Biophys Acta 2009; 1788: 768-778.
[79] Keane RW, Mehta PP, Rose B, Honig LS, Loewenstein WR and Rutishauser U. Neural differentiation, NCAM-mediated adhesion, and gap junctional communication in neuroectoderm. A study in vitro. J Cell Biol 1988; 106: 1307-1319.
[80] Meyer RA, Laird DW, Revel JP and Johnson RG. Inhibition of gap junction and adherens junction assembly by connexin and A-CAM antibodies. J Cell Biol 1992; 119: 179-189.
[81] Hertig CM, Eppenberger-Eberhardt M, Koch S and Eppenberger HM. N-cadherin in adult rat cardiomyocytes in culture. I. Functional role of N-cadherin and impairment of cell-cell contact by a truncated N-cadherin mutant. J Cell Sci 1996; 109: 1-10.
[82] Li J, Patel VV, Kostetskii I, Xiong Y, Chu AF, Jacobson JT, Yu C, Morley GE, Molkentin JD and Radice GL. Cardiac-specific loss of N-cadherin leads to alteration in connexins with conduction slowing and arrhythmogenesis. Circ Res 2005; 97: 474-481.
[83] Segretain D and Falk MM. Regulation of connexin biosynthesis, assembly, gap junction formation, and removal. Biochim Biophys Acta 2004; 1662: 3-21.
[84] Gwyn DG, Nicholson GP and Flumerfelt BA. The inferior olivary nucleus of the rat: a light and electron microscopic study. J Comp Neurol 1977; 174: 489-520.
[85] Sloper JJ and Powell TP. Gap junctions between dendrites and somata of neurons in the primate sensori-motor cortex. Proc R Soc Lond B Biol Sci 1978; 203: 39-47.
[86] Kosaka T. Gap junctions between non-pyramidal cell dendrites in the rat hippocampus (CA1 and CA3 regions). Brain Res 1983; 271: 157-161.
[87] Katsumaru H, Kosaka T, Heizmann CW and Hama K. Gap junctions on GABAergic neurons containing the calcium-binding protein parvalbumin in the rat hippocampus (CA1 region). Exp Brain Res 1988; 72: 363-370.
[88] Peters A, Palay SL and Webster HD. The Fine Structure of the Nervous System: Neurons and Their Supporting Cells. Third Edition. Oxford University Press; 1991.
[89] Kosaka T and Kosaka K. Neuronal gap junctions in the rat main olfactory bulb, with special reference to intraglomerular gap junctions. Neurosci Res 2003; 45: 189-209.
[90] Basu R, Taylor MR and Williams ME. The classic cadherins in synaptic specificity. Cell Adh Migr 2015; 9: 193-201.
[91] Friedman LG, Benson DL and Huntley GW. Cadherin-based transsynaptic networks in establishing and modifying neural connectivity. Curr Top Dev Biol 2015; 112: 415-465.
[92] Stocker AM and Chenn A. The role of adherens junctions in the developing neocortex. Cell Adh Migr 2015; 9: 167-174.
[93] Nishioka H, Mizoguchi A, Nakanishi H, Mandai K, Takahashi K, Kimura K, Satoh-Moriya A and Takai Y. Localization of l-afadin at puncta adhaerentia-like junctions between the mossy fi-

ber terminals and the dendritic trunks of pyramidal cells in the adult mouse hippocampus. J Comp Neurol 2000; 424: 297-306.
[94] Mizoguchi A, Nakanishi H, Kimura K, Matsubara K, Ozaki-Kuroda K, Katata T, Honda T, Kiyohara Y, Heo K, Higashi M, Tsutsumi T, Sonoda S, Ide C and Takai Y. Nectin: an adhesion molecule involved in formation of synapses. J Cell Biol 2002; 156: 555-565.
[95] Honda T, Sakisaka T, Yamada T, Kumazawa N, Hoshino T, Kajita M, Kayahara T, Ishizaki H, Tanaka-Okamoto M, Mizoguchi A, Manabe T, Miyoshi J and Takai Y. Involvement of nectins in the formation of puncta adherentia junctions and the mossy fiber trajectory in the mouse hippocampus. Mol Cell Neurosci 2006; 31: 315-325.
[96] Toyoshima D, Mandai K, Maruo T, Supriyanto I, Togashi H, Inoue T, Mori M and Takai Y. Afadin regulates puncta adherentia junction formation and presynaptic differentiation in hippocampal neurons. PLoS One 2014; 9: e89763.
[97] Sotelo C and Palay SL. The fine structure of the later vestibular nucleus in the rat. II. Synaptic organization. Brain Res 1970; 18: 93-115.
[98] Shapiro L and Weis WI. Structure and biochemistry of cadherins and catenins. Cold Spring Harb Perspect Biol 2009; 1: a003053.
[99] Harris TJ and Tepass U. Adherens junctions: from molecules to morphogenesis. Nat Rev Mol Cell Biol 2010; 11: 502-514.
[100] Miyahara M, Nakanishi H, Takahashi K, Satoh-Horikawa K, Tachibana K and Takai Y. Interaction of nectin with afadin is necessary for its clustering at cell-cell contact sites but not for its cis dimerization or trans interaction. J Biol Chem 2000; 275: 613-618.
[101] Takai Y and Nakanishi H. Nectin and afadin: novel organizers of intercellular junctions. J Cell Sci 2003; 116: 17-27.
[102] Takai Y, Ikeda W, Ogita H and Rikitake Y. The immunoglobulin-like cell adhesion molecule nectin and its associated protein afadin. Annu Rev Cell Dev Biol 2008; 24: 309-342.
[103] Mori M, Rikitake Y, Mandai K and Takai Y. Roles of nectins and nectin-like molecules in the nervous system. Adv Neurobiol 2014; 8: 91-116.
[104] Itoh M, Nagafuchi A, Yonemura S, Kitani-Yasuda T, Tsukita S and Tsukita S. The 220-kD protein colocalizing with cadherins in non-epithelial cells is identical to ZO-1, a tight junction-associated protein in epithelial cells: cDNA cloning and immunoelectron microscopy. J Cell Biol 1993; 121: 491-502.
[105] Mandai K, Nakanishi H, Satoh A, Obaishi H, Wada M, Nishioka H, Itoh M, Mizoguchi A, Aoki T, Fujimoto T, Matsuda Y, Tsukita S and Takai Y. Afadin: a novel actin filament-binding protein with one PDZ domain localized at cadherin-based cell-to-cell adherens junction. J Cell Biol 1997; 139: 517-528.
[106] Takahashi K, Nakanishi H, Miyahara M, Mandai K, Satoh K, Satoh A, Nishioka H, Aoki J, Nomoto A, Mizoguchi A and Takai Y. Nectin/PRR: an immunoglobulin-like cell adhesion molecule recruited to cadherin-based adherens junctions through interaction with Afadin, a PDZ domain-containing protein. J Cell Biol 1999; 145: 539-549.
[107] Shaw RM, Fay AJ, Puthenveedu MA, von Zastrow M, Jan YN and Jan LY. Microtubule plus-end-tracking proteins target gap junctions directly from the cell interior to adherens junctions. Cell 2007; 128: 547-560.
[108] Spruston N. Pyramidal neurons: dendritic structure and synaptic integration. Nat Rev Neurosci 2008; 9: 206-221.
[109] Alle H and Geiger JR. Combined analog and action potential coding in hippocampal mossy fibers. Science 2006; 311: 1290-1293.
[110] Holcman D and Yuste R. The new nanophysiology: regulation of ionic flow in neuronal subcompartments. Nat Rev Neurosci 2015; 16: 685-692.
[111] Vyleta NP, Borges-Merjane C and Jonas P. Plasticity-dependent, full detonation at hippocampal mossy fiber-CA3 pyramidal neuron synapses. Elife 2016; 5: e17977.
[112] Urban NN, Henze DA and Barrionuevo G. Revisiting the role of the hippocampal mossy fiber synapse. Hippocampus 2001; 11: 408-417.
[113] Fanselow MS and Dong HW. Are the dorsal and ventral hippocampus functionally distinct structures? Neuron 2010; 65: 7-19.
[114] Maggio N and Segal M. Unique regulation of long term potentiation in the rat ventral hippocampus. Hippocampus 2007; 17: 10-25.
[115] Papatheodoropoulos C and Kouvaros S. High-frequency stimulation-induced synaptic potentiation in dorsal and ventral CA1 hippocampal synapses: the involvement of NMDA receptors, mGluR5, and (L-type) voltage-gated calcium channels. Learn Mem 2016; 23: 460-464.
[116] Schreurs A, Sabanov V and Balschun D. Distinct properties of long-term potentiation in the dentate gyrus along the dorsoventral axis: influence of age and inhibition. Sci Rep 2017; 7: 5157.